Journal of Solid State Electrochemistry (2018) 22:637–656
https://doi.org/10.1007/s10008-017-3835-5

REVIEW

Electrochemical synthesis and properties of gold nanomaterials

I. Saldan[1] · O. Dobrovetska[2] · L. Sus[2] · O. Makota[2] · O. Pereviznyk[1] · O. Kuntyi[2] · O. Reshetnyak[1]

Received: 3 August 2017 / Revised: 13 November 2017 / Accepted: 14 November 2017 / Published online: 22 November 2017

Abstract
Approximately two decades ago, gold catalyst opened up a new view of their properties when they are introduced in the form of nanomaterials, since at that time, many approaches to preparation and use of gold nanoparticles started to be used in many practical applications. Today, the research activity relating to gold nanomaterials is becoming systematic and goes further to make connections between their surface structure, chemical and physical properties, and possible applications. Since electrodeposition is one of the most controllable methods used to prepare nanoparticles, nanowires, and nanoclusters of gold, the present review gives preference on their electrochemical synthesis. The relationship between catalytic activity, size, morphology and stability of gold nanomaterials is discussed in detail. Based on the properties of the prepared gold nanocatalysts, their new applications in chemical, photochemical, and electrochemical reactions have been observed.

Keywords Gold · Electrodeposition · Surface morphology · Size effect · Nanotechnologies

Introduction

Gold is a noble metal located in the 1B group of the periodic table and commonly considered as an inert and expensive material. In common aqueous solutions, it can exist in a number of oxidation states: (0), (+1), and (+3). Obviously, in vivo, gold might exist in an equilibrium between metallic gold and its oxidized states (+1) and (+3). On a macroscopic scale, zerovalent gold does not oxidize in air and has been found to be inert to strong alkalis and acids while gold in (+1) and (+3) oxidative states is relatively unstable, where value (+3) provides gold with a strong oxidizing ability to be reduced to value (+1) by reductants, for example thiols. Since Au^{3+} cations preferentially react with S- rather than O- and N- donors, Au^{+} cations can be stabilized by thiolate ligands.

The electrical behavior of gold colloidal dispersions in solutions encompasses Au nanoparticles (AuNPs) with surface charges caused by adsorption of small ions, surfactants, or polyelectrolytes and with consequent electrokinetic properties [1, 2]. Very small AuNPs stabilized by organothiolate ligand monolayers were common examples of the most subsequent direct voltammetry of metal nanoparticles [3]. This kind of gold nanomaterials (AuNMs), called monolayer-protected clusters (MPCs), was prepared by "Brust synthesis" reported by the Schiffrin laboratory [2]. The size-dependent electronic and structural properties of AuNMs on oxide supports are among the most fascinating examples that show important features of heterogeneous catalysis [4, 5]. When AuNMs size is around a few nanometers, they might be an effective oxidation catalyst [6–8]. For example, a threshold in the size of ~ 2 nm has been found in [9], above which AuNMs are completely inactive as catalysts for the epoxidation of styrene by molecular oxygen. This fact suggests that the catalytic activity of AuNMs arises from the size-dependent alteration of their electronic structure. Energy binding shift of 1.1 eV in the $4f_{7/2}$-electron of gold is observed mainly in case of larger AuNMs, while for AuNMs smaller than ~ 3 nm decreasing particle size was associated with an increase in the $3d$–electron density of gold atoms and the onset of reactivity with oxygen in the air [10]. Indeed, the size-dependent alteration of the electronic structure gives rise to unusual catalytic activity that has been experimentally confirmed for AuNMs on repeated occasions. But even today, reactivity on the nanoscale remains an important challenge for gold and also for other elements.

The AuNMs became active for many chemical reactions when stabilized in the form of nanoparticles attached to metal

✉ I. Saldan
saldanivan@gmail.com

[1] Department of Physical and Colloid Chemistry, Ivan Franko National University of Lviv, 6 Kyryla and Mefodia St., Lviv 79005, Ukraine

[2] Institute of Chemistry and Chemical Technologies, Lviv Polytechnic National University, 12 Bandery St., Lviv 79013, Ukraine

oxide and activated carbon supports [11–14]. This was started since the discovery of high catalytic activity for low-temperature CO oxidation in 1989 [15]. From that time on, researchers have been developing various methods to synthesize different types of AuNMs with controlled size and shape. As compared to chemical or physical methods, the electrochemical preparative and analytical procedures are cheap and diverse, and further investigations in this field are in continuous progress. This has led to fundamental research of their fascinating size-, shape-, and composition-dependent thermal, optical, and electrochemical properties.

Researches have also exploited small size, high surface area, and unique size-dependent properties for a range of applications, including sensing, separations, plasmonics, catalysis, nanoelectronics, therapeutics, biological imaging, and diagnostics. Additionally, for these applications, one more important issue is AuNMs' stability, that is not only their resistance against aggregation and size or shape transformations, but also inertness to oxidation and dissolution.

In the present review, a preference is made on electrochemical preparation of AuNMs. Surface functionalization by gold electrodeposition, morphology, and stability of AuNPs, gold nanowires (AuNWs), and gold nanoclusters (AuNCs) is discussed in detail. Size effect on gold reactivity and selectivity has been observed to be the main feature of AuNMs to be used in chemical reactions. New directions of gold application in nanotechnologies are predicted for the nearest future.

Surface functionalization by gold electrodeposition

As compared to palladium or platinum, gold has a lower melting point and a lower affinity for metal oxides. Therefore, AuNMs deposition as nanoparticles on metal oxide supports through impregnation methods looks difficult. Moreover, during calcination of dispersed $HAuCl_4$ crystallites, chloride ion markedly enhances the coagulation of AuNMs on the support surfaces. Therefore, it is very important to choose a suitable preparation method depending on the properties of support materials. Electrodeposition was found as a solution to prepare AuNMs on electrode surface of indium tin oxide (ITO), silicon, glassy carbon (GC), carbon nanotubes (CNs), and graphene (G).

Gold electrodeposition on ITO

As compared to bulk gold, AuNMs show better electrocatalytic activity for many electroactive species [16, 17]. ITO electrodes exhibit poor electrocatalytic activity, but favorably low and flat background current [18]; therefore, the modification of ITO electrodes with a low surface coverage of AuNMs could allow high electrocatalytic activity along with low background current. For the first time, the group of Prof. Compton [19] prepared gold nanoparticle that modified ITO-film-coated glass electrodes through direct electrochemical deposition from 0.5 M H_2SO_4 containing 0.1–1 mM $HAuCl_4$. AFM results directly confirmed around 70–300-nm gold nanoparticles (AuNPs) formed under different deposition time and $HAuCl_4$ concentration. In all cases, dispersed AuNPs were found on the electrode surface. Increase in the deposition time under applied electrodeposition resulted in a bigger average particle size of AuNPs, while higher concentration values led to higher number of seeds (nucleation) on the surface. Additionally, it was found that at pulse regime more uniform AuNPs might be obtained as compared to those at stationary power supply. The real surface area of the AuNPs electrodeposited on ITO film coated glass electrode (0.02–1 cm^2) was estimated on the basis of the amount of charge consumed during the reduction of Au_2O_3 monolayer and a reported value of 400 μC cm^{-2} was used for the calculation [20, 21]. Then, R. J. Forster et al. [22] electrodeposited gold island (< 100 nm) on a fluorine-doped ITO coated glass. Double potential step approaches coupled with interfacial engineering via monolayer formation allowed AuNPs to be created with controlled particle size, density, and particle size distribution in a reproducible manner. Group of R. J. Forster reported on the formation of gold nanodeposits using Penner's slow growth technique [23, 24] where the ability to control the nucleation mode, particle density, particle size, and particle size distribution by controlling the potentiostatic deposition conditions was described. Penner's group was a particular success using the application of a large overpotential nucleation pulse for a very short time (5–10 ms) followed by a longer lasting low overpotential growth pulse yielding particle size uniformity. Therefore, high overpotential nucleation pulse encourages instantaneous nucleation giving high particle density and also increasing particle size monodispersity. R. J. Forster et al. [22] used the 10–250-ms nucleation pulse applied to the fluorine-doped ITO-coated glass working electrode within the potential range of – (400–2000) mV, followed by a growth pulse at 300–700 mV until a set charge was passed. In addition to that, the effect of surface modification with a self-assembled monolayer 3-aminopropyldimethylmethoxysilane on the nucleation and growth kinetics was suggested since this approach can provide a more uniform surface electrodeposition process. Moreover, it was found that surface modification by amine groups altered the surface energy and kinetics of deposition on the surface making instantaneous nucleation possible at lower overpotentials, thereby reducing diffusion zone coupling. Similar surface modification was applied in [25], where 3-aminopropyltriethoxysilane was used to prepare amine-functionalized self-assembled monolayers on ITO electrodes. Amine groups protonated at neutral pH were readily bounded to a negatively charged metal complex. Hence, chemical reduction of such bound ions allows the facile formation of AuNPs on the amine-functionalized ITO surface through electrostatic

adsorption of $AuCl_4^-$ ions followed by chemical reduction. Without electrode surface modification, AuNMs looked like gold submicroparticles [26, 27], though their catalytic activity were successfully applied as a sensor to control refractive index for variety of organic solvents or quantity of CO. A new approach to gold nanoparticle electrodeposition with the help of ionic liquid at a three-phase junction was presented in [28]. The electrodeposition was carried out through inverted double-pulse potential chronoamperometry. Direct reduction of $AuCl_4^-$ ions at the electrode was followed by a counterion transfer through the liquid-liquid interface. As compared to electrodepositon from a single-phase, this method provided higher local surface coverage of angular AuNPs with narrow size distribution (110 ± 30 nm in diameter).

Silicon support for AuNPs

For the first time, large-area and high-density gold nanoparticle arrays with sub-10-nm gaps were synthesized on Si(100) substrate through electrochemical deposition with the application of an unusually high overpotential [29]. It was found that the extremely high overpotential contributes to the relatively small critical island size and high nucleation rate. A deep study of gold electrodeposition on a *n*-doped silicon substrate using different electrochemical techniques (cyclic voltammetry, square wave potential pulse, step potential, and step current) and conditions of variables (temperature, pH, reagent concentration, reaction kinetics, deposition time, etc.) was carried out in [30]. According to Osaka et al. [31], if the thiosulphate concentration is low in relation to the $[Au(S_2O_3)_2]^{3-}$ complex, the reaction mechanism consists of two steps:

$$2\left[Au(S_2O_3)_2\right]^{3-} \left(Au_2S_2O_3\right)_{ads} + 3\ S_2O_3{}^{2-} \quad (1)$$

$$\left(Au_2S_2O_3\right)_{ads} + 2\bar{e} \rightarrow 2\ Au + S_2O_3{}^{2-} \quad (2)$$

The former (1) implies adsorption of a neutral $(Au_2S_2O_3)_{ads}$ intermediate, while the latter (2), as the rate-determining step, is its electrochemical reduction to deposit gold with colloidal sulfur impurities.

$$\left[Au(S_2O_3)_2\right]^{3-} + \bar{e} \rightarrow Au + 2\ S_2O_3{}^{2-} \quad (3)$$

However, if the thiosulphate concentration is high in relation to the $[Au(S_2O_3)_2]^{3-}$ complex, the reaction (1) shifts towards the formation of the $[Au(S_2O_3)_2]^{3-}$ complex, and gold deposition takes place directly from the species in solution (3) without any intermediates [30]. It was concluded that the proposed mechanism for Au^+ reduction from the $[Au(S_2O_3)_2]^{3-}$ complex corresponded to a charge transfer of one electron without adsorbed intermediates, thus a sulfur-free gold deposit could be obtained. Additionally, it should be noted that, among all the electrochemical methods used, cyclic voltammetry method yielded the largest grain size gold deposits since because that electrodeposition took place at a very slow rate. The authors of [30] concluded that for any electrochemical method at a constant pH and temperature value the grain size in the diffusion regime is less comparable to electrodeposition process controlled by electron transfer under cation reduction. Since ionic diffusion increases with temperature both in solution and on the electrode surface, the grain size of the deposits is expected to be larger.

Recently, authors of [32] examined current transients for the reduction of aureate salts at the poorly doped *p*-type Si(100) photocathodes. They found that the hydrogen evolution reaction is significant even at very basic pH values, leading to a poor match between the modeled and actual outcomes in electrodeposition experiments. Finally, they concluded that the catalytic activity of AuNPs and semiconductor photo effects make it difficult to rely on current transients alone to refine the experimental conditions for the growth of AuNPs on Si(100) photocathodes. Therefore, it was proposed that hydrogen evolution might cause turbulence leading to the displacement of particles and significant aggregation on the surface. In order to avoid this problem, the gold electrodeposition with high overpotentials for hydrogen evolution was recommended. That allows control nucleation process and ultimately to use illumination patterns to spatially address AuNPs deposition on semiconducting surfaces.

Glassy carbon electrode for gold electrodeposition

A solution containing thiosulphate and sulphite was also developed for gold electrodeposition on a flat-plate GC electrode to study the mechanism of nucleation and crystal growth of gold nuclei [33]. It was found that at the early stages of the reduction process, the deposition process exhibited instantaneous nucleation of non-overlapping AuNPs. The electrodeposition on glassy carbon for 1 s resulted in uniform coverage of gold nuclei having a relatively uniform size of 80 ± 5 nm, while for 10 s, there could be observed some coalescence of gold crystals, and for 100 s, large aggregates with diameter within the range of 100–300 nm were obtained. At longer periods, the particles began to overlap and the deposition followed a classic progressive nucleation phenomenon. A simple one-step electrodeposition method was used to fabricate various gold nanostructures on GC electrodes in the 5 mM $HAuCl_4$ solution [34]. Hierarchical waxberry-like gold nanostructures with high active surface areas were obtained at pH 4, and they showed a higher catalytic performance for the reduction of oxygen than the other nanogold. These gold structures also displayed an extraordinary superhydrophobicity, and the contact angle increased with the increase of deposition temperature and time. It was concluded that the morphologies of AuNMs can be easily controlled by varying the pH and temperature value. The authors of [34] adjusted the pH of the $HAuCl_4$ solution,

and with the increase of the solution pH through NaOH addition, the color of the solution turned from yellow to nearly colorless. That change could be reversed through lowering the pH again by adding HCl. It is commonly believed that, with the pH increase, the Cl^- from a complex anion is displaced by water, and further hydrolysis and loss of proton from neutral hydrated ion occurs [35, 36]:

$$[AuCl_4]^- + H_2O \; AuCl_3(H_2O) + Cl^- \quad (4)$$

$$AuCl_3(H_2O) \; [AuCl_3(OH)]^- + H^+ \quad (5)$$

$$[AuCl_3(OH)]^- + H_2O \; AuCl_2(H_2O)(OH) + Cl^- \quad (6)$$

$$AuCl_2(H_2O)(OH) \; [AuCl_2(OH)_2]^- + H^+ \quad (7)$$

$$[AuCl_2(OH)_2]^- + H_2O \; [AuCl(OH)_3]^- + H^+ + Cl^- \quad (8)$$

$$[AuCl(OH)_3]^- + H_2O \; [Au(OH)_4]^- + H^+ + Cl^- \quad (9)$$

Finally, it was concluded that the pH value of gold precursor baths directly influenced existent forms of gold complex that resulted in a different redox potential and reduction rate of gold. In [37], a novel procedure for the fabrication of AuNPs assembled on GC via three consecutive steps—grafting of amino groups, anchoring of $[AuCl_4]^-$ ions by the $-NH_3^+$ groups, and electrochemical reduction of the $[AuCl_4]^-$ ions to the AuNPs—was applied in practice with a honeycomb-like configuration enriched in the Au (110) facet orientation. The oxygen reduction reaction as a sensitive reaction for the crystallographic orientation of the gold surface [38] was taken as a probing reaction to assign the facets of the prepared nano-Au/$-NH_2$/GC electrode in the O_2-saturated 0.5 M KOH. The observed quasi-reversible cyclic voltammetry response was characteristic of Au (111) and Au (110) single crystalline electrodes [38], therefore, taking into account reductive desorption measurements for Au (110) or Au (100) facets and excluding the Au (111) facet for bulk gold, it was concluded that the AuNPs of the nano-Au/$-NH_2$/GC electrode were enriched in the Au (110) crystallographic orientation. Recently, the group of prof. Compton scanned a AuNPs-modified GC macroelectrode in the 0.10 M HCl [39]. When gold loadings on the GC surface varied, the anodic peak charge increased linearly and indicated that 1.9 ± 0.1 electrons are transferred per one gold atom. The electrochemistry of gold in aqueous solutions in the presence of complex-forming anions was thoroughly studied, and chloride ions were found to facilitate its electrodissolution via formation of $[AuCl_4]^-$ and $[AuCl_2]^-$ complex ions:

$$Au + 4\,Cl^- \; [AuCl_4]^- + 3\,\bar{e} \quad (10)$$

$$[AuCl_4]^- + 2\,Au + 2\,Cl^- \; 3\,[AuCl_2]^- \quad (11)$$

It was found that anodic particle coulometry method can help identify AuNPs by reliability of the clear threshold potential for the onset of impact transients and its coincidence with the oxidation peak in the stripping voltammetry. The understanding of the anodic behavior of AuNPs in HCl enables us to explore the electrooxidation of single AuNPs in the same media via the anodic particle coulometry method through nanoparticle–electrode collisions. It was found that it agreed well with the size of 10.5 ± 1.0 mm for single particles, and it was clear that aggregation of AuNPs into gold clusters containing 2, 4, 8 single nanoparticles occurs on the experimental timescale. Development of a simple method for activating the GC surfaces with amino groups was proposed in [40], where AuNPs were further immobilized on the amine-terminated GC surfaces through electrostatic interaction, and then on the GC electrode, they were proven to facilitate the electron exchange between the electrode and the redox molecules in an aqueous solution (Fig. 1).

According to [41], electrodeposition of gold in GC/1 mM$[AuCl_4]^-$ with 0.1 M $HClO_4$ followed the Volmer-Weber growth mode. In the potential range of between 0.84 and 0.94 V, the electrodeposition kinetics related to progressive nucleation and diffusion-controlled growth of 3D AuNPs. It was found that at more negative electrode potentials than 0.64 V, the process of electrodeposition might occur under instantaneous nucleation. Therefore, AuNPs with a uniform size can be deposited applying the double-pulse technique involving an instantaneous nucleation pulse followed by a slow growth pulse. This fabrication strategy was proposed for other sp^2-bonded carbon materials such as CNs and G, opening up potential applications in the area of electrocatalysis due to its convenient preparation and suitable properties.

Carbon nanotubes modified by AuNPs

On the CNs surface chemical reduction of gold cannot be possible since the redox potential of any Au ion is lower than that of CNTs. In order to overcome this limit of the deposition, a process called substrate-enhanced electroless deposition was developed [42], where AuNMs might be spontaneously deposited onto the CNs, supported on a metal substrate with a lower redox potential than that of Au ions. Hence, the CNs are not the reducing agent in this method, and they only act as cathodes and templates for gold deposition. In common electrochemical deposition, CNs play a role of a molecular conducting wire and supports for AuNMs. The size of the electrodeposited nanoparticles and their distribution on the sidewalls of CNs can be controlled by the concentration of gold precursor and various electrochemical parameters, including nucleation potential and deposition time. The method of AuNMs electrochemical deposition on the CNs surface typically demonstrates a very fast nanoparticles formation, moreover with a high purity and adhesion to the CNs surface. Usually, electrochemically prepared AuNMs on CNs are characterized by a big particles size within the range of ~ 50–

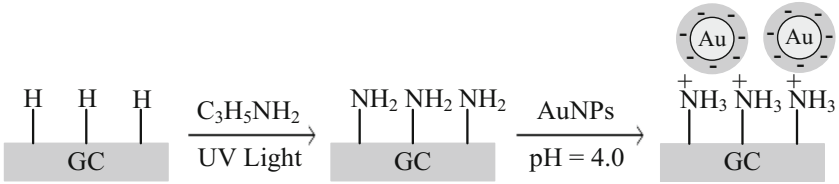

Fig. 1 Illustration of photochemical modification of the GC surface and subsequent attachment of AuNPs onto the GC surface. Adapted with permission from [40]. Copyright © 2010, Springer Science +Business Media, LLC

500 nm; therefore, it is a challenge to synthesize them of the size of a few nanometers with high dispersion on the CNs surface. A solution to this problem might be found due to a divergence between a larger driving force that is a more negative deposition potential, for critical nuclei formation and an inhibitive mechanism for deterring crystal growth under lower deposition charge or smaller current density [43]. In practical application, electrodeposition of AuNMs on CNs covered carbon paste electrode surface provided a significant enhancement of homocysteine oxidation signal [44]. This approach may offer an ultra-sensitive platform for biosensing thiol-containing molecules. Deposited AuNPs on the CN-modified electrode were able to produce the signal almost three orders of magnitude higher than a non-modified carbon paste electrode. A specific nanostructure of AuNMs might cause a high surface area and hence electrocatalytic properties for the modified electrode. Electrodeposited from $HAuCl_4$ AuNPs on the CN-modified electrode surface had a cauliflower-like morphology with ~ 200 nm in diameter, and that was the reason for high electrocatalysis for oxidation of ascorbic acid, dopamine, and uric acid [45]. Three electrochemical cyclic voltammogram scans of 0.25 mM of $HAuCl_4$ in the 0.1 M KNO_3 solution were analyzed in detail. For the first scan, a cathodic peak at 0.55 V and an anodic peak at 1.12 V (vs. Ag/AgCl) resulted from the reduction of Au^{3+} ions and the stripping of the electrodeposited gold, respectively. During the subsequent scans nucleation occurred at smaller overpotential (0.75 V), again resulting from reduction of Au^{3+} ions on the deposited gold nucleus at the first scan. The values of pulse potentials were obtained as − 0.1 V for nucleation and 0.75 V for growth pulse with 25 ms and 120 s duration, respectively.

Gold decoration for graphene layers

In 2008 G, that is a two-dimensional single layer of graphite, started to be actively modified by different noble metal nanoparticles, including AuNMs [46–49]. However, there are not too many publications concerning the loading of controlled or large amounts of AuNPs on graphene sheets [50–53]. Positively charged AuNPs with the size of ~ 2–6 nm were self-assembled on the surfaces of 1-pyrene butyric acid functionalized graphene sheets simply by mixing their aqueous dispersions under the driving force of electrostatic interaction. The amount of the AuNPs assembled on the modified G sheets could be easily modulated by controlling the feeding weight ratio of both components. Additionally, it was found that the modified G sheets had a high loading capability of AuNPs, and the maximum value was determined to be ~ 300 times higher than own weight of 1-pyrene butyric acid functionalized graphene sheets. The surface of GC electrodes, covered by this AuNMs-G composite, showed high electrocatalytic activity and electrochemical stability. A uric acid electrochemical sensor based on the composite modified electrode was proposed to get a rapid response and high sensitivity. Recently, a simple method of depositing uniform AuNPs on a less than 10 stacked layers of G coated with poly[2,2′-(2,6-pyridine)-5,5′-bibenzimidazole] without using any capping agents has been proposed in [54]. The AuNPs obtained, with the size of 1.6 ± 0.3 and 3.3 ± 0.5 nm, exhibited an excellent activity for oxygen reduction reaction, with the onset potential at − 0.11 and − 0.09 V (vs. Ag/AgCl), respectively.

AuNMs with different morphologies such as polygons, dendrites, irregular islands, and dense clusters have been obtained on the G surface in [55]. G samples were prepared on a silicon wafer with an insulating SiO_2 layer of 300 nm through micromechanical cleavage of natural graphite flakes. The 4-nm-thick layer of gold was thermally deposited on the G surface, where dense clusters of gold were prepared at room temperature [56, 57]; polygons and irregular islands of gold were formed at 100 and 80 °C, respectively; and gold dendrites appeared when the substrate was cooled down from 80 °C to the room temperature. The authors of [58] demonstrated a considerable effect of substrate temperature on the nucleation and growth of gold films through vapor deposition on single crystal graphite. As the temperature of substrate increases to or above 200 °C, the greater kinetic-controlled island growth results in much more prominent coalescence and grain growth events, so that more three-dimensional and geometrical metal islands can be observed. Based on the same principle, the observed morphologies of gold films on the G surface [55] agreed well with those shown on the graphite surface. Due to high temperature at the beginning of deposition, the nucleation of gold tends to be scattered and the saturated islands have a bigger size. But then temperature goes down and the atom mobility decreases. Therefore, the following AuNPs would choose a nearby growing island in the coalescence process and form a smaller island during

recrystalization. This approach results in the typical gold dendrites where big nuclei appear in the center, surrounded by small branches [55]. Additionally, it should be noted that the polygon of gold which consists of geometrical gold islands was prepared on a single layer graphene at a relatively low substrate temperature as compared to that of graphite. Thickness-dependent morphologies of gold thermally deposited onto the *n*-layer G were observed in [57], where the highest density of gold particles on monolayer graphene was attributed to its highest surface diffusion barrier through *n*-layer G. It was concluded that with the substrate staying at a higher deposition temperature, the shift in the surface free energy or the surface diffusion barrier within G is more prominent, therefore morphologies of gold films are expected to change more easily on G than on graphite.

Morphology and stability of AuNMs

Definitely, the size and shape of the deposited AuNMs should be controlled by the conditions created, where deposition time and concentration of a gold precursor were the first responsible factors [59]. However, temperature value had a more multipurpose influence on the surface morphology. Since nucleation density and the deposition rate increase, when the applied temperature increases, the grain size of the deposit decreases. Obtained at 60 °C, AuNMs displayed dense and homogeneous microstructures with spherical particles, and the deposited layer was a bit stressed stripe [60]. This fact might be explained by the appearance of internal or residual stress during electrodeposition of metals or alloys. The stress can originate from intrinsic film stress and from interfacial stress between the deposit and the substrate [61]. Additionally, in the wet chemistry synthesis certain surface active substances or buffers might affect the nucleation stage and hence control the shape of gold nanoclasters, nanoislands, and nanoparticles. Zwitterionic buffer, 2-[4-(2-hydroxyethyl) piperazin-1-yl] ethanesulfonic acid used in [62] acted as a reducing and shape-directing agent yielding irregular AuNPs. This irregular particles morphology with corners and edges supported a higher surface density of incipient gold oxide that might act as a fast redox mediator for the oxidation of glucose, while regular spherical morphology of AuNPs was minimally active. In contrast to photonic applications that typically require uniform nanoparticles, the electrocatalysis was successfully completed with a number of gold aggregates of different shapes and sizes.

Nanoporous gold film

It is well-known that electrodes with multimodal pore size distribution on the nano- or micrometer scale are desirable for most applications. The presence of micro-pores promotes the fast transportation of the reactants while nanopores are a reason for a high surface area and hence increase the rate of the chemical or electrochemical reaction. High surface area gold could be prepared through electrochemical dealloying [63], or through electrodeposition within rigid templates [64]. Such electrodes usually have a uniform pore size distribution, this frequently resulting in insufficient electrocatalytic and sensing performance. Moreover, porous metals prepared by dealloying often contain some amount of a less noble metal. Direct electrodeposition of nanoporous gold with controlled multimodal pore size distribution with the help of a dynamic hydrogen template was reported in [65]. Porous gold was prepared by electrodeposition from an aqueous electrolyte consisting of 0.1 M $HAuCl_4$ and 0–3 M NH_4Cl. Gold was potentiostatically deposited within the range of $E = 0$ to − 8 V (vs Ag/AgCl) on a Pt/Ti/Si electrode over 15–120 s. The gold foams were free impurities and had pore size in value of ~ 0.01–10 μm (Fig. 2). Roughness factor values (the ratio of real surface area to the geometric surface area) were estimated as 400–500. It was concluded that the deposition of porous gold foams is only possible when a sufficient amount of NH_4Cl is added to the electrolyte as a hydrogen source. The stabilized gold foams had a well-known structure on the nanoscale with ligaments, which are usually obtained after dealloying. Nanoporous gold prepared using this hydrogen templated electrodeposition method is very promising for electrocatalytic and sensing applications.

Reductive electron transfer dynamics in the multilayer film of alkanethiolate monolayer-protected AuNCs in contact with an aqueous electrolyte was studied in [66]. It was determined that electrons are transported within the film phenomenologically via the diffusion-like hopping between the localized protected AuNCs sites (Fig. 3) with an average first order rate constant of 10^4 s^{-1}. This value is comparable to those with a similar kind of films immersed in organic electrolytes but much smaller than those for the all-solid films. It was found that the solvent swelling produces a negligible effect on the electron hopping dynamics and that the electron transfer is most likely limited by the diffusive redistribution of the counterions in order to keep local electroneutrality.

Nanoporous gold film composed of three-dimensional bicontinuous nanostructures with a large surface area was prepared in [67]. Electrochemical cleaning process was applied to create a nanoporous gold electrode within the potential range from − 0.2 to + 1.6 V vs. a saturated calomel electrode in 1 M H_2SO_4 until stable cyclic voltammograms were obtained. Nano-channels inside the film provided ideal local environment for immobilization of enzyme molecules with expected stabilization of protein molecules. It was concluded that nanoporous gold electrodes offer microenvironments for redox molecules that are efficient in enzyme voltammetry as well as for mediated enzyme electrocatalysis. This behavior

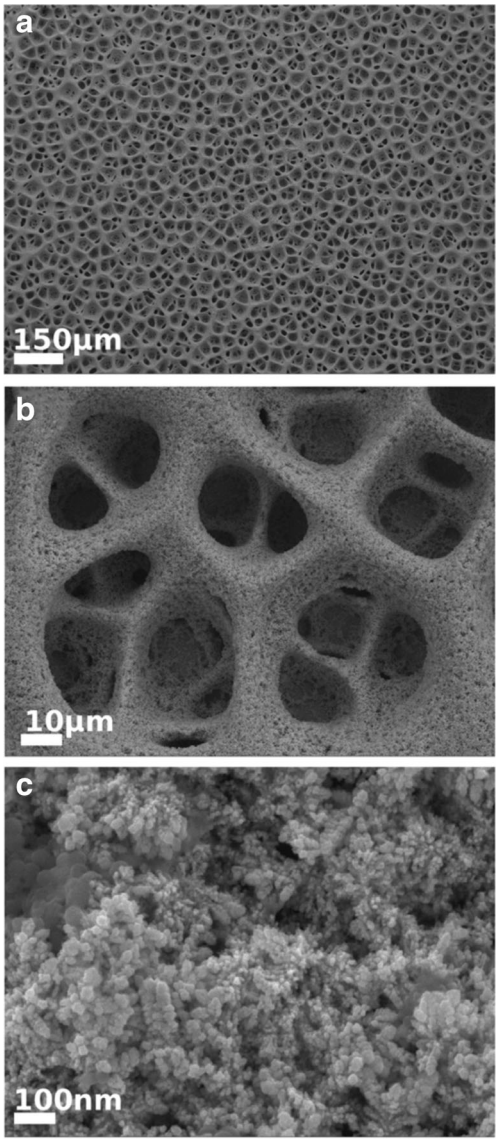

Fig. 2 SEM images of a typical multimodal gold foam electrodeposited at $E = -4$ V vs Ag/AgCl, $[NH_4]^+ = 2$ M, $t = 20$ s. Peprinted with permission from [65]. Copyright © 2010, Elsevier. B.V. All rights reserved

was explained by the obtained pore/ligament surface structure of the film as well as by the presence of areas of low-index Au(111), Au(100), and Au(110) surface structures. Moreover, these well-defined regions of the surface structured gold were reflected in clearly distinct anodic voltammetric peaks. Nanoporous gold films with different pore size were fabricated by chemical dealloying, where Ag-Au alloy in the form of the foil was immersed in 67% HNO_3 at room temperature for 24 h [68]. For some samples, anneal process at 200 °C for 2 h was applied afterwards. Excellent electrical conductivity as a notable advantage of the obtained films encouraged to use these AuNMs in the enzyme electrode construction. Therefore, nanoporous gold films were a success in catalysis and bio-sensoring.

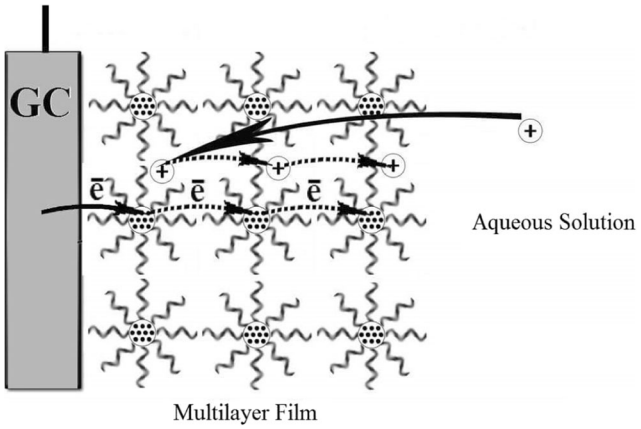

Fig. 3 Illustration of charging coupled by cation and electron migration (solid arrows) and the electron hopping between neighboring monolayers of protected AuNCs coupled by diffusive counterion relocation (dotted arrows). Adapted with permission from [66]. Copyright © 2012, Elsevier. B.V. All rights reserved

Formation of AuNWs

Anisotropic AuNPs, including nanowires, were synthesized applying several wet chemical approaches. Uniform gold nanorods with a controlled aspect ratio were prepared through electrochemical reduction in the presence of rod-shaped concentrated cationic surfactants called soft templates [69]. Rod- or thread-like surfactant micelles can be used to prepare gold nanorods through chemical and photochemical reduction [70]. Several groups have shown that the addition of Ag^+ ions to the gold growth solution constitutes an important factor in controlling the aspect ratio of gold nanorods [71]. Polycrystalline rod-shaped gold particles were prepared through electrochemical reduction in hard templates such as mesoporous Al_2O_3 or polycarbonate membranes [72]. More recently, seed-mediated crystal growth has been used in the synthesis of uniform gold nanorods, in which the seed concentration appears to be critical for shape-selective AuNWs formation [73]. Simple photochemical synthesis to prepare long, freestanding, and continuous AuNWs was developed in [74] (Fig. 4).

In the procedure, the addition of spherical seeds or silver ions was not applied, and it might be performed at ambient conditions. The ratio of $(AuCl_4)^-$ to cationic surfactant, hexadecyltrimethylammonium bromide, and the pH of the solution used for the growth played important roles in the AuNWs formation with aspect ratios more than 100. The solution with reactants was mixed for 10 s and then irradiated with 365 nm UV light for about 9 h at the distance of 10 cm from the light source, at room temperature. The color of the pure $HAuCl_4$ solution was light yellow, while the solution containing $HAuCl_4$ and hexadecyltrimethylammonium bromide became dark yellow. However, the color of the solution might be restored again to light yellow after the addition of certain amounts of NaOH. During UV irradiation, the solution irreversibly changed to a violet color with a blue tint, resulting

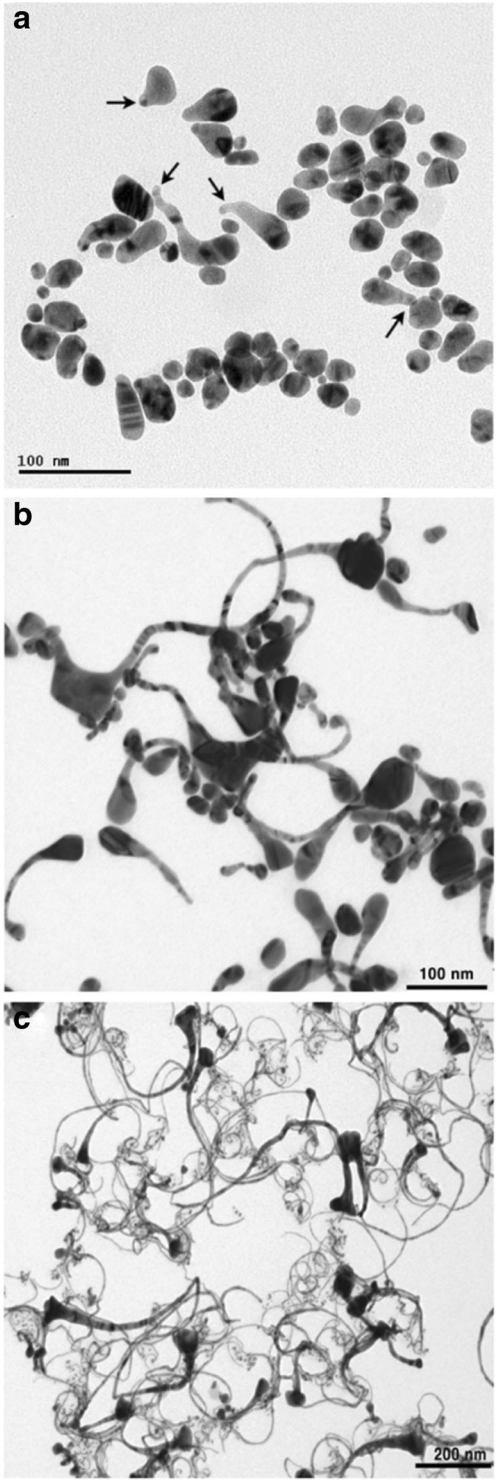

Fig. 4 TEM images of the gradual evolution of AuNWs during UV irradiation for 3 h (**a**), 6 h (**b**), and 9 h (**c**). Tadpole-shaped AuNPs are indicated with arrows in **a**. Peprinted with permission from [74]. Copyright © 2006, Korean Chemical Society

in a new absorption band appearing at around 530 nm, which corresponds to the well-known surface plasmon absorption band of gold nanocrystals. Facile synthesis of single crystalline AuNWs through reduction of $HAuCl_4$ in oleic acid and oleylamine was proposed in [75]. These micrometer-long wires were prepared with controlled diameters of either 3 or 9 nm. Moreover, the diameter could be further changed by varying the volume ratio between oleylamine and oleic acid. The linked 9-nm AuNWs showed high electron conductivity with the resistivity value of 260 Ω × nm, breakdown current of 250 μA and failure current density of 3.5×10^{12} A/m^2. It was concluded that those chemically synthesized single crystalline AuNWs might be used for molecular-scale interconnection in nanoelectronics. In [76], water-soluble AuNWs were prepared through the introduction of a trace amount of hydrophobic molecules (toluene or chloroform) to the gold precursor solution, using cylindrical hexadecyltrimethylammonium bromide micelles as templates. The mechanism of AuNWs synthesis was proposed on the basis of the soft template approach (Fig. 5).

Toluene or chloroform preferably incorporate with inner hydrophobic chains of the hexadecyltrimethylammonium bromide double layer, thereby leading to a decrease in the inner diameter of self-assembled cylindrical micelles, which in turn template the growth of the ultrathin AuNWs. It was concluded that such a simple and robust method can be extended onto the synthesis of a large variety of nanowires that get rich in hexadecyltrimethylammonium bromide as the surface capping ligands. Furthermore, the ability to create such ultrathin AuNWs may open up exciting opportunities for fundamental studies of their unique physical properties and hence promising applications in nanoscale photonic, electronic, and optoelectronic devices.

Size and structure of AuNCs

Many experiments and calculations have established that reactivity of metallic nanoclusters in gas-phase reactions varies with the number of atoms and with the charge on the atomic clusters. The chemistry of Me_n differs from that of Me_{n-1} or Me_{n+1} and obviously from that of Me_n^+ or Me_n^-. Therefore, it was assumed that nanoclusters supported on an oxide surface may have novel and interesting catalytic properties that are totally different from those of nanoparticles (diameter size in range of ~ 10–100 nm). In [77], it was summarized that (1) a change of the atomic number in a nanocluster alters its catalytic properties; (2) small cluster size limits the number of reactions on the nanocluster, which increase selectivity; (3) as compared to nanoparticles, a nanocluster is more sensitive to the nature of the support and environment; (4) catalytic properties of a nanocluster change more drastically when it is alloyed; (5) promoter or poisons affect nanoclusters more dramatically; (6) nanocluster changes its properties when exposed to charge donors or acceptors; and (7) when the catalyst is an expensive metal, the use of its nanoclusters is a benefit from the economic point of view. At the same time, some drawbacks were also identified and summarized as follows:

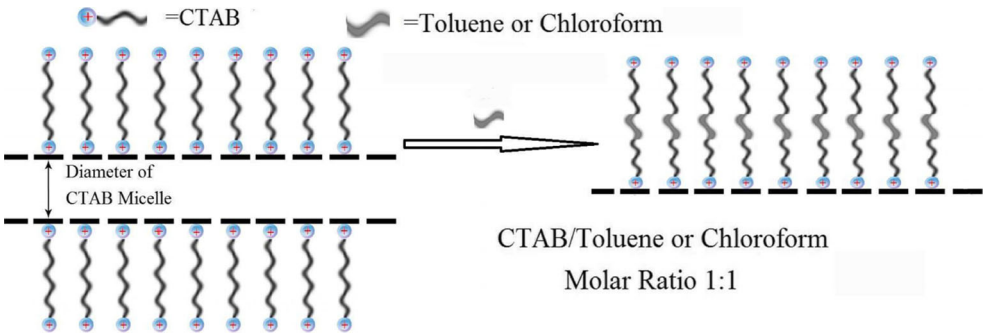

Fig. 5 The proposed mechanism for the formation of AuNWs. CTAB means cetyltrimethylammonium bromide. Adapted with permission from [76]. Copyright © 2015, The Royal Society of Chemistry

(1) from the thermodynamic point of view, the surface energy of a nanocluster decreases and hence an ensemble of nanoclusters coarsens to form nanoparticles with non-uniform size distribution; (2) the proposed controlled syntheses of nanoclusters is too expensive for practical use. In spite of that, AuNCs have come to be among the most convenient AuNMs to provide some correlations between structure and properties that can be extrapolated onto the respective nanoparticles used in practical catalysts.

Using electrochemical approaches, a unique advantage to form metal clusters at electrode surfaces might be found since the supersaturation is determined by the applied potential [78]. Thus, transient and relaxation methods can be used for studying the kinetics of cluster growth. However, in these experiments, the presence of a solid substrate can influence strongly the properties of the new deposited phase. Therefore, water/organic solvent (so called "liquid/liquid") interfaces offer an ideal substrate for the investigation of metal cluster nucleation phenomena by reducing or completely eliminating the interaction between the substrate and deposits. In experimental work [79, 80], it was shown that electron transfer between redox species present in immiscible water and organic phases can be observed by applying a suitable interfacial potential difference. To achieve this, the redox couples must be chosen such as to ensure that no ionic transfer reaction coupled to electron transfer occurs. The interest in these systems is that although no metallic phase is present as a substrate, electron transfer between the two phases, both containing ionic solutions, can be controlled by the applied Galvani potential difference. Electrochemical metal-cluster formation can be investigated when one of the components of the redox couple is an aqueous metal ion or a complex with a hydrophobic ligand L soluble in the organic phase, according to the reversible reactions [78]:

$$M^{z+}(w) + z\ \mathrm{Red}(o) \leftrightarrow M_z^{\sigma} + z\ \mathrm{Ox}(o) \tag{12}$$

or

$$[ML_x]^{z+}(o) + z\ \mathrm{Red}(w) \leftrightarrow M_z^{\sigma} + z\ \mathrm{Ox}(w) + xL(o) \tag{13}$$

where Red and Ox refer to the reduced and oxidized forms of the redox couples; M^{z+} represents the metal ion and M_z^{σ} is the metal particle formed at the interface containing z metal atoms; (w) and (o) refer to water and organic solvent, respectively. It is well-known that during metal electrodeposition, the supersaturation Gibbs energy (ΔG_s) for new phase formation and growth is obtained as follows:

$$\Delta G_s = -nF\eta \tag{14}$$

where n is the number of the transferred electrons and η is the overvoltage. For a reaction at the immiscible electrolyte solution interface, η value might be calculated as follows [78]:

$$\eta = \Delta_o^w\phi - \Delta_o^w\phi_{eq} \tag{15}$$

where $\Delta_o^w\phi$ and $\Delta_o^w\phi_{eq}$ is the applied and equilibrium Galvani potential difference for the two-phase reaction, respectively, which includes the standard potentials and activities of the two redox couples in their corresponding phases [79, 80]. First time, the AuNCs and their further coalescence to metallic films was successfully prepared electrochemically at the interface between two immiscible electrolyte solutions under a controlled applied potential [78]. The $AuCl_4^-$ anions were electrochemically reduced to AuNCs at the "liquid/liquid" interface and the interfacial growth of AuNPs with time was analyzed by in situ spectrophotometry.

AuNCs are metal atomic clusters consisting of groups of gold atoms, which have established compositions and stable geometric structures and usually have a diameter size of a few nanometers. Atomic clusters might be considered as the most elemental Au^0 building blocks (after separate gold atoms) bringing new possibilities for novel nano- or microstructure construction. The properties of AuNCs are very different from bulk gold, this offering their application in novel nanotechnologies such as sensors, biological labeling, electronics, and catalysis. Although synthesis and characterization of AuNCs is more difficult than that of the common AuNPs, their unique physical and chemical properties encouraged to pay attention to them in many scientific domains. The discovery of the fact that AuNCs are less toxic than classical semiconductors (e.g., CdS, GaAs, etc.) and that AuNMs become semiconductors when their dimensions are below ~2–3 nm results in a novel strategy of highly fluorescent and nontoxic gold quantum dots. Catalysis using AuNCs is of extensive interest not only in fundamental studies but also in practical applications.

Tsunoyama et al. [81] have studied the effect of electronic structures of Au-poly(*N*-vinylpyrrolidone) clusters on aerobic oxidation catalysis, when catalytic activity becomes higher with the decrease in the core size. One of the first chemical syntheses of AuNCs was a two-step top-down approach consisting in thiol-etching of AuNPs [82]. The bottom-up strategic approach shown here is a simple one-step electrochemical process, with biocompatible poly(*N*-vinylpyrrolidone) being used as a capping-stabilizing agent. AuNCs were synthesized in acetonitrile through modification of the electrochemical technique used before for AuNPs production [83, 84]. A new electrochemical method of producing fluorescent and paramagnetic Au-poly(*N*-vinylpyrrolidone) clusters was presented in [85] and showed several advantages, such as reproducibility and effectiveness, with a good control of the cluster size at the same time. Serious changes in fluorescent and magnetic properties were observed with only one-atom difference between the AuNCs, which can be easily predicted by the simple spherical Jellium model. The model proposed that Au_3 clusters should have the following electronic structure ($1S^2 2P^1$) and therefore exhibit a paramagnetic behavior that is contrary to Au_2 clusters ($1S^2$) which should display a diamagnetic behavior. Results of electron paramagnetic resonance measurements agreed well with theoretical calculations [86] showing that gold dimers (Au_2 clusters) have zero magnetic anisotropy energy while trimer (Au_3) is poorly magnetic, with the value of magnetic anisotropy energy of 8 meV only. Different conditions of electrochemical synthesis such as temperature value, time, and potential of gold nucleation were crucial for obtaining clusters with 2 or 3 gold atoms [87]. All those prepared in [85] AuNCs were very stable against strong reducing and oxidizing agents since no changes in their optical properties were observed during 2 years. Thermal stability of AuNCs with the size range of 4–6 nm in highly oriented pyrolytic graphite nanopits of well-defined depth was studied in [88]. At intermediate coverage, these AuNCs arranged themselves to form beads with constant density and narrow size distribution. The spacing between these beads varied within the range of 3.9–5.6 nm depending on the gold loading. The height of the AuNCs was independent from the pit depth, i.e., the number of fixing dangling bonds. These AuNCs were stable against thermal annealing under ambient conditions up to 750 K. Moreover, at higher temperatures, the size distribution became sharper, indicating particular stability for a given size. It was noticeable that AuNCs catalyzed the etching of the graphene layers and formed channels which have identical depths as the initial confining pits. Theoretical calculation of energy structures of AuNCs started for neutral gold clusters with atomic number from 2 up to 20 [89–92] and predicted the 2D → 3D transition point for neutral Au_{11} claster that drops in between that of cationic Au_8^+ and anionic Au_{12}^- AuNCs.

In practice, AuNCs must be stabilized by a stabilized agent (solution or substrate). But even at successful synthesis of a stabilized gold nanocluster, its structural study is still a big challenge due to the difficulty in growing gold single crystals for X-ray crystallography experiments. In this context, X-ray spectroscopy techniques such as X-ray absorption spectroscopy (XAS) and X-ray photoelectron spectroscopy (XPS) were found to be desirable alternative tools [93, 94] to analyze the structure and properties of, e.g., gold-thiolate nanoclusters [95]. The last experimental work included X-ray spectroscopy studies of the gold-thiolate nanoclusters, such as Au_n (n = 19;25;36;38). It was demonstrated that synchrotron-based XAS and XPS techniques were unique and powerful tools for probing the structural and electronic properties of the gold-thiolate nanoclusters. Using electrochemical deposition of AuNCs on ultrathin overoxidized polypyrrole film covering the surface of the GC electrode, a composite nanoelectrode array sensor was fabricated [96]. The AuNCs were electrochemically deposited under cyclic voltammetry scanning from 0.2 to − 1.0 V in the 0.5 mM $HAuCl_4$ solution at the scan rate of 50 mVs^{-1} for 15 cycles. Due to the synergic effect of the overoxidized polypyrrole film and AuNCs, the modified electrode had good stability, sensitivity, and selectivity to determine epinephrine and uric acid in the presence of ascorbic acid in large amounts. The catalytic activity of the overoxidized polypyrrole film was significantly enhanced by the presence of AuNCs, due to increased electronic conductivity and effective surface area. AuNCs were electrodeposited on the phosphorus incorporated tetrahedral amorphous carbon electrode and characterized by XPS, chronoamperometry, and cyclic voltammetry [97]. Two cycles of voltammogram of this electrode in the 0.5 mM $HAuCl_4$ solution at 0.02 Vs^{-1} (Fig. 6) showed similar curve shape as it was in [98]. Peak "A" of gold reduction was observed at about 0.16 V in the first scan, while peak "B" at − 0.30 V was related to the reduction of hydrogen ions to hydrogen atoms adsorbed on the electrode surface [99]. Peak "C" at 1.14 V on the returning curve confirmed oxidation of the electrodeposited AuNCs. A crossing of forward and reverse currents was observed

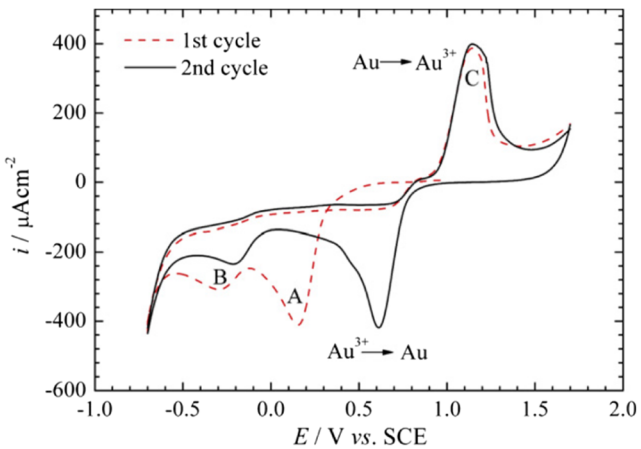

Fig. 6 Two cycles of voltammogram of the phosphorus incorporated tetrahedral amorphous carbon electrode in the 0.1 M H_3BO_4 + H_2SO_4 solution including 0.5 mM $HAuCl_4$ (pH = 1.4) at 0.02 Vs^{-1}. Reprinted with permission from [97]. Copyright © 2008, Elsevier. B.V. All rights reserved

at 0.81 V, and that fact was related to the equilibrium potential of Au/Au^{3+} electrochemical reaction. Peak "A" in the second cycle shifted to a more positive potential of 0.61 V that might be explained by the fact that already existent gold nuclei made the further gold deposition easier. Peak "B" also moved towards more positive potential values indicating a decrease in the overpotential for hydrogen reduction. Furthermore, the reduction and oxidation peak of gold shifted cathodically and anodically, respectively, with increasing sweep rate and a linear relationship between the maximum current at the peaks and the square root of sweep rate, suggesting that reduction and oxidation processes of AuNCs were diffusion-controlled. The size of AuNCs was controlled through alteration of the deposition time, representing progressive nucleation and diffusion-controlled growth of separate 3D gold islands. Significant enhancement of electrochemical activity and reversibility towards ferricyanide oxidation reaction was observed after AuNCs deposition on the surface of the tetrahedral amorphous carbon electrode that was proposed as a potential material to be used in electroanalysis.

Redox properties of monolayer-protected AuNCs were studied through cyclic voltammetry in polar organic solvents, where significant effect of electrolyte ions was observed [100]. A charging response bridging those demonstrated in aqueous and organic media was displayed. The overall charging process was kinetically controlled through electron hopping between the monolayer-protected AuNCs inside the film, which was thermodynamically coupled by the concurrent migration of supporting electrolyte counterions for electroneutrality. This valuable data is helpful for understanding why the counterion dependent redox charging was evident only in highly polar aqueous media but not in weakly polar or nonpolar organic solvents. A non-enzymatic electrochemical sensor using AuNCs to detect organophosphorus pesticides was proposed in [101]. Voltammetry scanning studies along with scan rate effect revealed a mixed mass transport regime where the thin layer diffusion effects exhibited the enhanced activity of the AuNCs. This fact might be explained by the high surface-to-volume ratio, large binding sites, and electronic effect. The proposed sensor matrix was evaluated employing square wave voltammetry, showing a very low detection limit of 0.65 nM for reductive methyl parathion detection. The authors of [101] experimentally confirmed that usage of AuNCs ion on the modified electrodes exhibited their suitability for enhanced and sensitive determination of methyl parathion as compared to bulk gold or even AuNPs.

Size effect of AuNMs on chemical reactivity and optical properties

Approximately one decade ago, scientists started giving the answer to the question as follows: "why are the actual size, shape and surface distribution of AuNMs interrelated and show a dependent influence on the physical and chemical properties of gold modified materials?" And the first issue in order to understand this behavior was controlled synthesis of AuNMs with desired parameters.

Controlled synthesis of AuNMs

Today, the pulsed electrodeposition technique remains the universal method for preparation of AuNMs with certain properties. According to the theory of nucleation [102], the size and number of nuclei depend on the overvoltage (η):

$$r = \frac{2\sigma V}{ze_0|\eta|} \tag{16}$$

where r means a critical nucleation radius, σ specific surface energy, V atomic volume in the crystal, and z the number of elementary charges e_o. High-nucleation density on the electrode surface can be achieved at a high η value. This high overvoltage can only be maintained for a few ms since cation concentration in the vicinity of the cathode decreases, and therefore, the process becomes diffusion-controlled [103]. Over the intervals between pulses (t_{off}), metal ions diffuse from the bulk electrolyte to the cathode and compensate metal ion depletion, and due to exchange current processes energetically more preferred larger crystallites grow at the expense of smaller crystallites. This process can be prevented by surface active substances that work as grain refiners when added directly to the electrolyte. In experimental work [104], it has been shown that current density, pulse duration, bath temperature, and composition were utilized for the variation of the crystallite size of AuNPs. The authors observed a decrease in the crystallite size down to 16 nm through proper choice of current density and temperature, and further down to 7 nm with the help of sulfur- or arsenic-containing additives. The grain growth kinetics of AuNPs was evaluated in terms of the growth model with size-dependent impediment. The value of activation energy of grain growth in nanocrystalline gold is considerably lower than that for grain boundary self-diffusion in coarse-grained gold. Using wet chemistry approach, the authors of [105] found that under similar synthetic conditions, a refined change of the thiolate ligand structure could have a significant effect on the resulting size of AuNCs. During the first step of synthesis, a polydispersed crude product protected by *para*-, *meta*-, *ortho*--methylbenzenethiol was prepared (Fig. 7). At this stage, 0.4 mmol of $HAuCl_4$ was phase-transferred from an aqueous solution to toluene using tetraoctylammoniun bromide (0.46 mmol), and then Au(III) was reduced to Au(I) through addition of the corresponding thiol (2 mmol), and eventually reduced to neutral AuNCs by NaBH4 (4 mmol). During he second step, the polydispersed crude product was subjected to size-focusing through etching with excess thiols at 80–90 °C without oxygen exclusion. Thus, the final products were obtained, and the formulas were determined

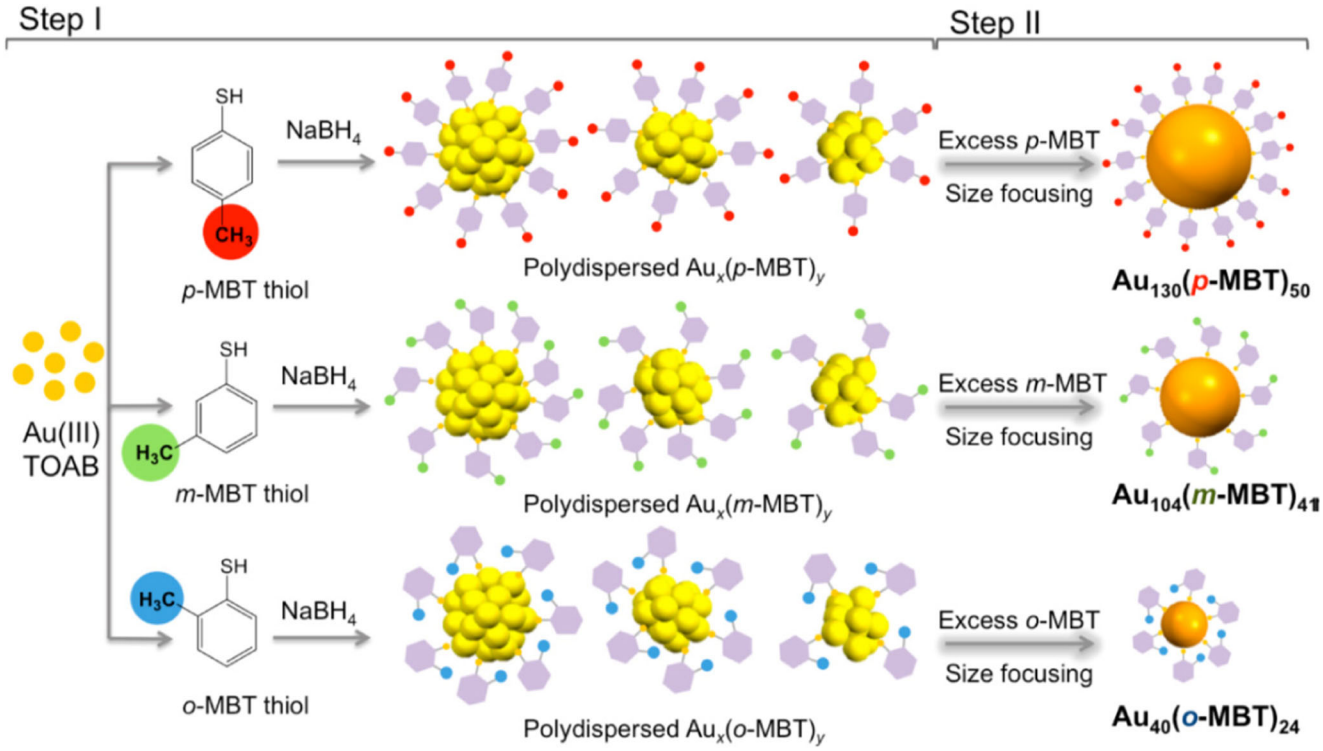

Fig. 7 The scheme of a two-step size-focusing synthesis of the ligand-stabilized gold nanocluster with size exploring *para*-, *meta*-, *ortho*-methylbenzenethiol (*p*-MBT, *m*-MBT, *o*-MBT) isomeric ligands. TOAB stands for tetraoctylammoniun bromide. Reprinted with permission from [105]. Copyright © 2015, American Chemical Society

to be Au_{130}(*para*-methylbenzenethiol)$_{50}$, Au_{104}(*meta*-methylbenzenethiol)$_{41}$, and Au_{40}(*ortho*-methylbenzenethiol)$_{24}$. The decreasing size sequence was in line with the increasing number of methyl group obstacles to the interfacial Au–S bond. The authors of [105] explained the shrinkage of the gold nanocluster sizes by the difference in the steric hindrance among the three isomeric methylbenzenethiols, where the closer the methyl group to the sulfur atom in the thiol, the more structural obstacles would occur in the gold-sulfur interface. Additionally, the authors concluded that the size and structure of AuNCs became sensitive to the refined structural change of protecting thiols only when the thiolate ligand backbone was rigid, otherwise a flexible ligand backbone would not show this influence on the nanoclusters size. This conclusion made clear why phenylethylthiol, aliphatic thiols, and glutathione showed similar nanoclusters sizes, despite their different ligand structures. Nevertheless, there is no answer to how the exact number of gold atoms in Au_n should be predicted through such wet chemical synthesis. It is suggested that depending on the thermodynamic stability of polydispersed crude product and the nature of the ligands, a certain size of AuNCs might be obtained. Therefore, stability of the final size of nanoclusters was a combination of the surface-protecting ligand and the core structure of AuNCs.

Another wet chemistry approach was used to synthesize AuNPs protected by pamoic acid [106]. The synthesized AuNPs capped by pamoic acid were used as seeds to prepare larger AuNMs [107]. The prepared seed solution was added to a mixture of $HAuCl_4$ and di-sodium salt of pamoic acid under stirring for 24 h to complete the growth of AuNPs. It was found that the size of the prepared AuNPs was changeable within the range of ~ 11–76 nm depending on the pH value, 8.1–3.7, respectively. Moreover, different sizes of AuNPs were also achieved through a seed-mediated growth approach. The fluorescence emission spectra of AuNPs protected by pamoic acid [107] showed significantly higher intensities and higher values of zeta potential, i.e., higher colloidal stabilities as compared to those of citrate-capped AuNPs [108].

Size effect on optical properties of AuNCs

The most striking example of fluorescence occurs when the radiation absorbed is within the ultraviolet region of the spectrum, and thus invisible for the human eye, while the emitted light is within the visible region, which gives the fluorescent substance a distinct color that can only be seen when exposed to UV light. In most cases, during fluorescence the emitted light has a longer wavelength, and therefore lower energy, than the radiation absorbed. As it has been mentioned before, depending on the values of zeta potential of gold colloids, the

intensity of fluorescence emission spectra might be different. However, the main peculiarity of gold from the optical point of view is the presence of electronic interband transitions within the visible range; hence, absorbed specific light energies might yield their distinct color. Plasmons that might be considered as collective oscillations of the free electron gas density have a great effect on the optical properties of AuNMs. The light of frequencies below the plasma frequency is reflected by AuNPs because the electrons in the material screen the electric field of the light. AuNPs are of great huge interest due to their distinctive optical property known as surface plasmon resonance (SPR) [109]. Additionally, based on the laser-induced SPR supported by AuNMs conventional surface-enhanced Raman scattering might appear. Since localized surface plasmons (LSPs) are charge density oscillations confined to metallic nanoparticles, the excitation of LSPs by incident light results in the appearance of intense surface plasmon (SP) absorption band, which is affected by the changes in the refractive index of nanoparticle proximity [110].

Localized surface plasmon resonance (LSPR) of twin-linked AuNPs deposited onto transparent ITO was used as a label-free optical biosensor of an enzyme [111]. LSPR excitation was found to depend on the particle alignment, interparticle distance, and excitation wavelength [112]. It was shown that periodic gold nanoparticle arrays exhibited a fast third-order nonlinear optical response [113]. Aggregated AuNPs in hydrophobic poly(etherimide) membranes demonstrated three-photon type nonlinear absorption attributed to excited state absorption occurring in nanostructures [114]. The authors of [115] decided to study third harmonic generation abilities of 20–50 nm AuNPs covalently attached to the ITO substrate, and particular influence of size dispersion on the output optical and nonlinear optical effects was studied. It was expected that the effects of the size of AuNPs could be explored without leading to irregularity of AuNPs. Using the hyperfine AFM methods including the surface topology, three types of samples which are different by size were identified. It was concluded that by size and shape AuNPs were highly monodispersed, with a defined interparticle distance. The prepared nanoparticles together with their separation from the conducting ITO substrate were found to be the minimum criterion for their use as materials for perfect interactions with external electromagnetic light and laser coherence in particular. The authors of [115] found a substantial increase in at least two spectral peaks of the photo-induced absorption and showed that this process continued after interruption of the laser dealing. There were three bands observed within the photo-induced absorption spectra of AuNPs located on the ITO situated at about 350, 430, and 580 nm. The first band at about 350 nm was attributed to the interband recombination of the valence *d*-band electrons with the holes in the *sp.*-band conducting. At the same time, a drastic increase in the third harmonic generation during decreasing of nanoparticles' size from 50 to 20 nm was found, which fact may be accounted for by localized nano-confined effects.

Size effect on selectivity and catalytic activity of AuNMs

Catalysis by AuNMs has become one of the fastest growing research topics in the field of catalysis [116, 117]. AuNPs in close vicinity to substrates showed high activity and selectivity in a number of chemical reactions, including low-temperature CO oxidation and propylene epoxidation [13], selective hydrogenation of unsaturated hydrocarbons [118], etc. AuNPs of smaller size generally showed higher alcohol conversion, due to their increased number of exposed gold atoms, although controversial results were reported with regard to the size effect based on per surface atom or per unit surface area of gold [119]. This behavior might be due to strong interaction between AuNPs and the substrate. It might be concluded that carbon-supported AuNPs exhibited higher activity for glycerol or glycol oxidation than oxide-supported catalysts [120], suggesting dependence of the gold catalytic activity on the substrate composition [121]. Other studies revealed that AuNPs supported by metal oxides (e.g., CeO_2, TiO_2) could also show high catalytic activity for oxidation of aliphatic and aromatic alcohols [122]. Moreover, in the aerobic oxidation of aliphatic alcohols, activity of AuNPs supported by the CeO_2 substrate was significantly enhanced through reduction of the particle size of CeO_2 [123].

Ethanol oxidation over AuNPs immobilized on the SiO_2 substrate gave acetic acid and acetaldehyde as the main products [116]. Ethyl acetate was identified as the only by-product due to a minor esterification reaction between ethanol and acetic acid. It was found that selectivity to acetic acid was counter-related with that to acetaldehyde and the level of ethanol conversion appeared to be the sole factor in determining the product selectivity, independent of the AuNPs size. The selectivity to acetaldehyde was close to 100% when the ethanol conversion was less than 3%. When the level of ethanol conversion increased, selectivity to acetaldehyde gradually decreased with an attendant increase in selectivity to acetic acid, and hence the overall reaction gradually shifted from acetaldehyde to acetic acid selective catalytic process. The areal activity of the AuNPs of ~ 5 nm immobilized on the SiO_2 substrate was found to be higher than either smaller (~ 3 nm) or larger (~ 10–30 nm) Au particles. Further study of the dependence of product yields on ethanol conversion demonstrated that oxidation reaction proceeded by the same reaction mechanism over these differently sized AuNPs, in which acetaldehyde was formed as the intermediate reaction product to acetic acid.

The particle size effects of AuNPs on oxygen reduction in the acidic medium have been studied in [124]. AuNPs were chemically prepared with controlled size distributions (1.7 ±

0.5, 4.8 ± 2, and 13.2 ± 2 nm) and deposited onto a carbon support. In the case of bulk gold, the number of electrons involved in oxygen reduction reaction (z) was nearly constant at the potential above − 0.2 V, while the increase of z value was observed for AuNPs of less than 10–15 nm and the potential shifted to a more negative value, indicating that activity of the 2-step 4-electron reduction was high or even the direct 4-electron reduction of O_2 to H_2O occurred. The maximum increase of z value was observed when the size of the AuNPs was less than 3 nm. The Au/SiO_2 system was characterized by SEM, Auger electron spectroscopy and thermal desorption for gaseous CO [125]. Initial adsorption probability, which quantifies zero coverage reactivity of AuNPs towards adsorption of CO gas-phase species, versus gold exposure curves showed the maximum for AuNCs with the size of ~ 3.5 nm. In [126], Au/C catalysts containing AuNPs with the size ≤ 4.7 nm had the highest mass activities during glycerol oxidation and were at least twice as active as those with the size ≥ 43 nm. But AuNPs with the size of ~ 2 nm were not stable since they demonstrated growth during repetitive cycling in KOH. The catalysts containing small AuNPs also showed lower glycerol oxidation onset potentials than those with large AuNPs, corresponding to their activation at lower potentials. The lower onset potentials could be related to the predominance of Au(110) facets on small AuNPs while large AuNPs were also poisoned possibly due to a higher fraction of Au(111) or a lower gold surface area showing an early decline in glycerol oxidation currents, within the region where gold should still be active. While the mass activity trend favored small AuNPs due to the influence of the particle size on the specific surface area, larger AuNPs were found to manifest higher specific electrocatalytic activity for glycerol oxidation, i.e., to be free from surface area effects. It was noted that from the practical point of view factors like mass activity, lower overpotentials and higher stability were most relevant, and these conditions for fuel cell application could all be met by small AuNPs with predominantly Au(110) facets.

Direct measurements of peak potential for electrochemical oxidation of AuNPs attached to the ITO electrode as a function of the particle size was described in [127]. AuNPs arrays with particle diameters within the range of 8–250 nm through electrodeposition of Au from $HAuCl_4$ in H_2SO_4 at potentials of − 0.2 to 0.8 V vs Ag/AgCl using chronocoulometry to keep constant amount of deposited gold were synthesized. The average AuNPs size increased with the increase in the deposition potential. Another approach using chemical reduction of $HAuCl_4$ by $NaBH_4$ in trisodium citrate solution led to ~ 4 nm average diameter of AuNPs which were chemisorbed to the ITO electrode. Linear sweep voltammograms obtained on the gold-decorated ITO electrodes with the constant coverage of gold in terms of Au atoms per square centimeters and with the particle size from 4 to 250 nm from 0.5 to 1.1 V in 0.01 M KBr and 0.1 M $HClO_4$ showed a positive shift in the oxidation potential from 734 ± 1 to 913 ± 19 mV with the increase in the AuNPs size. The shift agrees qualitatively well with the one predicted by a shift in the redox potential based on the difference in free energy associated with the change in the surface energy as a particle size function. On the basis of the charge during gold deposition versus the charge during oxidation, oxidation process produces a mixture of $AuBr_4^-$ (25%) and $AuBr_2^-$ (75%) anions:

$$Au^0 + 2\,Br^- \rightarrow AuBr_2^- + \bar{e} \qquad E^0\left(Au^{+1}/Au^0\right) = 0.963\ V\ vs\ NHE \tag{17}$$

$$Au^0 + 4\,Br^- \rightarrow AuBr_4^- + 3\,\bar{e} \qquad E^0\left(Au^{+3}/Au^0\right) = 0.858\ V\ vs\ NHE \tag{18}$$

In practice, the ITO electrode coated with a mixture of 4 and 250 nm AuNPs revealed two oxidation peaks consistent with the two AuNPs size populations presented on the surface. In [128], a dramatic negative thermodynamic shift in the oxidation potential for < 4 nm AuNPs was reported. On the basis of the Plieth equation [129], the lowest oxidation potentials were calculated for AuNPs with the diameter within the range of 1–2 nm:

$$E_{\mathrm{NPs}} = \left(-\frac{2\gamma V_{\mathrm{m}}}{zF}\right)\left(\frac{2}{d}\right) + E_{bulk} \tag{19}$$

where E_{NPs} and E_{bulk} were the oxidation potential of AuNP and bulk gold, respectively; γ was the surface tension; V_{m}, molar volume; z and F, the number of electrons and Faraday's constant, respectively; and d, the AuNP diameter. Additionally, it was shown that together with reaction (13, 14) gold can be oxidized through chemical reaction (20) [39]:

$$Au^0 + AuBr_4^- + 2\,Br^- \rightarrow 3\,AuBr_2^- \tag{20}$$

Finally, it was summarized that "3ē" electrochemical oxidation through reaction (14) was thermodynamically favorable, although previously an average "1.5ē" [128] and "1.9ē" [39] electrochemical oxidation was reported. Today, the reaction mechanisms of gold oxidation through reactions (17), (18), and (20) are not yet understood; however, the experimental data best agrees with those calculated by Plieth equation for a process involving "1ē" or an average of "1.5ē" electrons. This fact suggests that because of a huge difference in the surface energy value between AuNCs with the size of 1–4 nm and common AuNPs with the size of 10–100 nm, the value of the activation energy should be different, thus affecting the reaction mechanism. Obtained in [128], experimental results suggested that oxidation of the smallest AuNCs in the presence of Br^- or Cl^- showed less dependence on the halide nature while for common AuNPs, it was highly prominent. It can be concluded that today only two main properties of AuNMs are definitely established in the

"AuNCs → AuNPs" direction, and these are lower reactivity and higher colloidal stabilities.

Modern applications of AuNMs

The supported AuNMs showed remarkable structure sensitivity during their usage in catalysis because of low activation energy values. According to [130], developments on gold catalyst are expected in three directions: (i) the first direction involves the discovery of new capabilities for AuNPs (with the size of 10–50 nm); (ii) the second direction is the study of the catalytic reaction mechanism of AuNMs; and (iii) the third direction involves the research works on AuNCs (with size of 1–3 nm). Today, the chemistry of gold starts being rich. Numerous ino- and organic compounds of gold were synthesized to become suitable precursors for AuNMs synthesis [131]. Single-crystal gold surfaces were used as model catalysts or electrodes for surface science or electrochemical studies and as substrates for the construction of self-assembled monolayers [132]. Preparation and characterization of ligand-protected AuNPs or AuNCs revealed a great attention paid to them due to their practical applications in catalysis/electrocatalysis. Homogeneous catalysis by soluble gold complexes and heterogeneous catalysis by supported AuNMs have become new frontiers in modern catalysis [133]. Since the time when Haruta and coworkers reported that supported AuNPs exhibited astonishing activity in CO oxidation below room temperature [15], heterogeneous catalysis by AuNMs has been paid a considerable attention to from the theoretical and experimental points of view. The main reactions studied to date based on gold heterogeneous catalysis are well-known gas-phase reactions with a wide practical application:

$$CO + {}^{1}/_{2}\, O_2 \rightarrow CO_2 \quad (21)$$

$$CO + H_2O \rightarrow CO_2 + H_2 \quad (22)$$

$$CH_4 + 2\, O_2 \rightarrow CO_2 + 2\, H_2O \quad (23)$$

$$H_2 + O_2 \rightarrow H_2O_2 \quad (24)$$

More than 2000 relevant papers have been published in this area including development of novel AuNMs, elucidation of the nature of active sites and performance of kinetics studies on gold. This fact stimulated an increasing number of publications dealing with the non-conventional synthesis of AuNMs catalysts. In [134], it was found that reaction mechanism of supported AuNPs for low-temperature CO oxidation (17) was highly dependent on the nature of the support. The catalytic active sites on the reducible metal oxide-supported gold mainly positioned at the interfaces of gold and the support where CO and O_2 molecules might be adsorbed, activated, and finally react'. Factors that could change the length of the perimeters between gold and the reducible metal oxide substrate, including the size and structure of AuNPs and the morphology of the support material could greatly influence the catalytic performance of the nanocatalyst. Other words supporting gold further confirmed that the boundary between gold and the support was considered as the active site. Catalytic activity of gold supported by irreducible oxide supports was mainly attributed to low coordinated gold atoms. Thus, in wet chemistry or electrochemical synthesis of AuNMs, respectively, the stabilizing agent or supporting material plays an important role in the catalytic activity of gold. For example, the thiolated chitosan derivative successfully acted as a reduction and capping agent for AuNPs, and these materials showed fast catalyzed reduction of methylene blue [135]. Therefore, the extended concept for the stabilizing ligands or support materials would shed some light on the catalytic mechanism for catalysis through AuNMs [136–138].

Many factors can influence electrocatalytic activities of AuNP-modified ITO electrodes [139]. Using surface plasmon absorption spectra of AuNP-modified electrodes, it was found that the decreased gold activity is not induced by AuNPs aggregation or their desorption from the electrode. Some reports have shown that hydrogen ad- or absorption into gold generates strain in metal lattices, which induces structural change and results in metastable and highly active surface states [140]. These states remain even after hydrogen removal, and AuNPs activation was proposed through $NaBH_4$ or cathodic treatment [141]. However, in [139], it was confirmed that highly active surface states might be generated during preparation of AuNPs, and they might be converted into less active surface states via slow structural reorganization. Taking into account valuable results from [139–141], AuNPs might be considered as catalyst under hydrogen absorption-desorption in metal-hydride electrodes based on Ti-Ni alloys [142–144]. However, in order to fully exploit the potential application of AuNPs in electrochemistry, perfect AuNMs with well-defined properties and long-term stability in various environments have to be designed. Other attractive AuNMs in the form of disks, plates, sponges, stars, flakes, urchins, prisms, wires, and rods are the focus of intensive research [145–148]. When the properties of these AuNMs are combined with modern electrochemical technology, a more novel and sensitive interface will be constructed, which fact will result in a more profound nanoelectrochemistry development. Additionally, AuNMs are widely used in electroanalytical studies and have good capacity to prepare electrochemical sensing platforms with high sensitivity and selectivity to detect target molecules on the basis of different analytical strategies. In [145], it was shown that AuNPs and inorganic nanomaterials could be used as enhanced electrode materials for electrochemical sensing applications. A reasonable combination of different inorganic nanomaterials with good conductivity may open up a new approach to gold-decorated hybrid nanomaterials as reinforced elements for the construction of a high performance

electrochemical sensor [149]. This is due to the fact that composite nanomaterials could provide larger electrochemically active surface areas for the adsorption of target molecules and effectively accelerate electron transfer between electrode and detection molecules [150–153]. In order to improve sensitivity and selectivity of colorimetric sensors, engineering AuNPs with functional molecules having high recognition ability is required. Today, a significant research interest is directed towards AuNP-based colorimetric assays for DNA, enzyme activity, small molecules, metal ions, carbohydrates, and proteins, with their unique SPR being used as sensing elements [154–160]. Especially, DNA-functionalized AuNPs as sensing elements have become of greater interest since DNA has many unique functions which could be easily adjusted by the target molecules binding. Research results on AuNMs reveal that their modern application in catalysis can open up many good opportunities in an extremely multidisciplinary environment, for them to be used as a catalyst in chemical-, photochemical-, and electrochemical reactions.

Conclusions

Today, the research of AuNMs is intensive and will help open up new methods to control their properties, hence stimulate their novel application in catalysis. One of the current challenges for AuNMs is either their very high activity or stability. Therefore, screening of a special design of these nanomaterials to provide both high catalytic activity and durability has developed in some directions. The first is to design monodisperse AuNCs with rich high-index facets. The second is to synthesize multimetallic NPs with diverse morphologies and compositions. And the third is to find connection between the surface properties of advanced supports and controllable size, shape and microstructure of AuNMs. Based on chemical and physical properties of AuNMs, their application is found far beyond as a catalyst in a typical chemical reaction. In electrocatalysis pure AuNMs and, specially, AuNMs combined with another component can provide specific surface reaction centers of predictive properties [161]. Additionally, because of their biocompatibility, medical applications become very attractive using the combination of AuNPs core with attached functional groups. Usage of AuNMs as drug delivery systems in photodynamic therapy for cancer treatment opens unusual advantages by the incorporation of photosensitiser ligands in plasmonic AuNPs [162]. Since AuNCs can be catalytically active in chemical, photochemical and electrochemical reactions, they might be considered as universal NMs to catalyze many complex physical, chemical and biomedical processes.

Acknowledgements Dr. O. Makota acknowledges assistance in the online library received within the frame of DAAD scholarship (reference number 91574246).

Funding information The authors thank for financial support obtained from the national project of the Ministry of Science and Education of Ukraine (project number ХФ-56Ф).

References

1. Schmid G (1992) Large clusters and colloids. Metals in the Embryonic State Chem Rev 92:1709–1727
2. Brust M, Walker M, Bethell D, Schiffrin DJ, Whyman R (1994) Synthesis of thiol-derivatised gold nanoparticles in a two-phase liquid-liquid system. J Chem Soc Chem Commun 7:801–802
3. Murray RW (2007) Nanoelectrochemistry: metal nanoparticles, nanoelectrodes, and nanopores. Chem Rev 108:2688–2720
4. Santra AK, Goodman DW (2003) Oxide-supported metal clusters: models for heterogeneous catalysts. J Phys Condensed Matter 15: R31–R62
5. Daniel MC, Astruc D (2004) Gold nanoparticles: assembly, supramolecular chemistry, quantum-size-related properties and applications toward biology, catalysis and nanotechnology. Chem Rev 104:293–346
6. Haruta M (1997) Size- and support-dependency in the catalysis of gold. Catalys Today 36:153–166
7. Sau TK, Pal A, Pal T (2001) Size regime dependent catalysis by AuNPs for the reduction of eosin. J Phys Chem B 105:9266–9272
8. Cortie MB, Van der Lingen E (2002) Catalytic gold nano-particles. Mater Forum 26:1–14
9. Turner M, Golovko V, Vaughan O, Abdulkin P, Berenguer-Murcia A, Tikhov M, Johnson B, Lambert R (2008) Selective oxidation with dioxygen by gold nanoparticle catalysts derived from 55-atom clusters. Nature 454:981–983
10. Miller JT, Kropf AJ, Zha Y, Regalbuto JR, Delannoy L, Louis C, Bus E, van Bokhoven JA (2006) The effect of gold particle size on Au–Au bond length and reactivity toward oxygen in supported catalysts. J Catalys 240:22–234
11. Bond GC, Thompson DT (1999) Catalysis by gold. Catal Rev Sci Eng 41:319–388
12. Haruta M, Date M (2001) Advances in the catalysis of Au nanoparticles. Appl Catal A 222:427–437
13. Haruta M (2002) Catalysis of gold nanoparticles deposited on metal oxides. CATTECH 6:102–115
14. Haruta M (2003) When gold is not noble: catalysis by nanoparticles. Chem Record 3:75–87
15. Haruta M, Yamada N, Kobayahsi T, Iijima S (1989) Gold catalysts prepared by coprecipitation for low-temperature oxidation of hydrogen and of carbon monoxide. J Catal 115:301–309
16. Aiken JD, Finke RG (1999) A review of modern transition-metal nanoclusters: their synthesis, characterization, and applications in catalysis. J Mol Catal 145:1–44
17. Biswas PC, Nodasaka Y, Eyno M, Haruta M (1995) Electrooxidation of CO and methanol on graphite-based platinum electrodes combined with oxide-supported ultrafine gold particles. J Electroanal Chem 381:167–177
18. Aziz MA, Park S, Jon S, Yang H (2007) Amperometric immunosensing using an indium tin oxide electrode modified with multi-walled carbon nanotubeand poly(ethylene glycol)–silane copolymer. Chem Commun 25:2610–2612
19. Dai X, Compton RG (2006) Direct electrodeposition of AuNPs onto indium tin oxide film coated glass: application to the detection of arsenic(III). Anal Sci 22:567–570

20. Kozlowska HA, Conway BE, Hamelin A, Stoicoviciu L (1987) Elementary steps of electrochemical oxidation of single-crystal planes of Au Part II. A chemical and structural basis of oxidation of the (111) plane. J Electroanal Chem 228:429–453
21. Trasatti S, Petrii OA (1991) Real surface area measurements in electrochemistry. Pure Appl Chem 63:711–734
22. Sheridan E, Hjelm J, Forster RJ (2007) Electrodeposition of AuNPs on fluorine-doped tin oxide: control of particle density and size distribution. J Electroanal Chem 608:1–7
23. Penner RM (2002) Mesoscopic metal particles and wires by electrodeposition. J Phys Chem B 106:3339–3353
24. Liu H, Penner RM (2000) Size-selective electrodeposition of mesoscale metal particles in the uncoupled limit. J Phys Chem B 104: 9131–9139
25. Aziz MA, Patra S, Yang H (2008) A facile method of achieving low surface coverage of au nanoparticles on an indium tin oxide electrode and its application to protein detection. Chem Commun 14:4607–4609
26. Wang Y, Deng J, Di J, Tu Y (2009) Electrodeposition of large size AuNPs on indium tin oxide glass and application as refractive index sensor. Electrochem Commun 11:1034–1037
27. Wang JY, Diao P, Zhang DF, Xiang M, Zhang Q (2009) Electrochemical sensing of CO by gold particles electrodeposited on indium tin oxide substrate. Electrochem Commun 11:1069–1072
28. Kaminska I, Niedziolka-Jonsson J, Roguska A, Opallo M (2010) Electrodeposition of AuNPs at a solid|ionic liquid|aqueous electrolyte three-phase junction. Electrochem Commun 12:1742–1745
29. Fang J, You H, Ding B, Song X (2007) Large-area and high-density gold nanoparticle arrays with sub-10 nm gaps. Electrochem Commun 9:2423–2427
30. Gamero M, Alonso C (2010) Deposition of nanostructurated gold on n-doped silicon substrate by different electrochemical methods. J Appl Electrochem 40:175–190
31. Osaka T, Kato M, Sato J, Yoshizawa K, Homma T, Okinaka Y, Yoshioka O (2001) Mechanism of sulfur inclusion in soft gold electrodeposited from the thiosulfate-sulfite bath. J Electrochem Soc 148:659–662
32. Vogel YB, Darwish N, Kashi MB, Gooding JJ, Ciampi S (2017) Hydrogen evolution during the electrodeposition of gold nanoparticles at Si(100) photoelectrodes impairs the analysis of current-time transients. Electrochim Acta 247:200–206
33. Martínez-Paredes G, Begoña González-García MB, Costa-García A (2010) Genosensor for detection of four pneumoniae bacteria using gold nanostructured screen-printed carbon electrodes as transducers. Sensor Actuator B 149:329–335
34. Zhang H, Xu J, Chen H (2008) Shape-controlled gold nanoarchitectures: synthesis, superhydrophobicity and electrocatalytic properties. J Phys Chem C 112:13886–13892
35. Guo ZR, Zhang Y, Huang L, Wang M, Wang J, Sun JF, Xu LN, Gu N (2007) One-step controlled synthesis of anisotropic gold nanostructures with aniline as the reductant in aqueous solution. J Colloid Interface Sci 309:518–523
36. Moreau F, Bond GC, Taylor AO (2005) Gold on titania catalysts for the oxidation of carbon monoxide: control of pH during preparation with various gold contents. J Catal 231:105–114
37. Othman SH, El-Deab MS, Okajima T, Ohsaka T (2009) Novel procedure for the fabrication of gold nanostructures enriched in Au (110) facet orientation. Electrochem Commun 11:1273–1276
38. Arihara K, Ariga T, Takashima N, Arihara K, Okajima T, Kitamura F, Tokuda K, Ohsaka T (2004) Multiple voltammetric waves for reductive desorption of cysteine and 4-mercaptobenzoic acid monolayers self-assembled on gold substrates. Phys Chem Chem Phys 5:3758–3761
39. Zhou YG, Rees NV, Pillay J, Tshikhudo R, Vilakazi S, Compton RG (2012) Gold nanoparticles show electroactivity: counting and sorting nanoparticles upon impact with electrodes. Chem Commun 48:224–226
40. Zhou Y, Zheng X, Wu L, Zhi J, Xu M (2011) An easy method for manufacture of AuNPs on a glassy carbon surface. J Mater Sci 46: 1139–1142
41. Komsiyska L, Staikov G (2008) Electrocrystallization of Au nanoparticles on glassy carbon from $HClO_4$ solution containing $[AuCl_4]^-$. Electrochim Acta 54:168–172
42. Qu LT, Dai LM (2005) Substrate-enhanced electroless deposition of metal nanoparticles on carbon nanotubes. J Am Chem Soc 127: 10806–10807
43. Wu B, Kuang Y, Zhang X, Chen J (2011) Noble metal nanoparticles/carbon nanotubes nanohybrids: synthesis and applications. Nano Today 6:75–90
44. Hung VWS, Kerman K (2011) Gold electrodeposition on carbon nanotubes for the enhanced electrochemical detection of homocysteine. Electrochem Commun 13:328–330
45. Afraz A, Rafati AA, Najafi M (2014) Optimization of modified carbon paste electrode with multiwalled carbon nanotube/ionic liquid/cauliflower-like gold nanostructures for simultaneous determination of ascorbic acid, dopamine and uric acid. Mater Sci Eng C 44:58–68
46. Mastalir A, Kiraly Z, Patzko A, Dekany I, L'Argentiere P (2008) Synthesis and catalytic application of Pd nanoparticles in graphite oxide. Carbon 46:1631–1637
47. Muszynski R, Seger B, Kamat PV (2008) Decorating graphene sheets with gold nanoparticles. J Phys Chem C 112:5263–5266
48. Si YC, Samulski ET (2008) Exfoliated graphene separated by platinum nanoparticles. Chem Mater 20:6792–6797
49. Varns R, Strange P (2008) Stability of gold atoms and dimers adsorbed on grapheme. J Phys Condens Matter 20:225005
50. Hong W, Bai H, Xu Y, Yao Z, Gu Z, Shi G (2010) Preparation of gold nanoparticle/graphene composites with controlled weight contents and their application in biosensors. J Phys Chem C 114: 1822–1826
51. Zhu L, Liu Y, Yang P, Liu B (2015) Label-free aptasensor based on electrodeposition of gold nanoparticles on graphene and its application in the quantification of adenosine triphosphate. Electrochim Acta 172:88–93
52. Farquhara AK, Brooksbya PA, Dryfe RAW, Downard AJ (2017) Controlled electrodeposition of gold nanoparticles onto copper-supported few-layer graphene in non-aqueous conditions. Electrochim Acta 237:54–60
53. Yiwei X, Wen Z, Jiyong S, Xiaobo Z, Yanxiao L, Tahir HE, Xiaowei H, Zhihua L, Xiaodong Z, Xuetao H (2017) Electrodeposition of gold nanoparticles and reduced graphene oxide on an electrode for fast and sensitive determination of methylmercury in fish. Food Chem 237:423–430
54. Fujigaya T, Kim CR, Hamasaki Y, Nakashima N (2016) Growth and deposition of Au nanoclusters on polymer-wrapped graphene and their oxygen reduction activity. Sci Rep 6:21314
55. Qiu C, Zhou H, Cao B, Sun L, Yu T (2013) Raman spectroscopy of morphology-controlled deposition of Au on graphene. Carbon 59:487–494
56. Lee J, Shim S, Kim B, Shin HS (2011) Surface-enhanced Raman scattering of single- and few-layer graphene by the deposition of AuNPs. Chem Eur J 17:2381–2387
57. Zhou HQ, Qiu CY, Liu Z, Yang HC, Hu LJ, Liu J, Yang H, Gu C, Sun L (2010) Thickness-dependent morphologies of gold on N-layer graphenes. J Am Chem Soc 132:944–946
58. Wayman CM, Darby TP (1975) Nucleation and growth of gold films on graphite: II. The effect of substrate temperature. J Cryst Growth 28:53–67

59. Chu L, Han L, Zhang X (2011) Electrochemical simultaneous determination of nitrophenol isomers at nano-gold modified glassy carbon electrode. J Appl Electrochem 41:687–694
60. Wei L, Kai D, Lin Z, Jiang X, Chao Z, Yunwang Z, Lan Z, Qiang Y (2013) Electrochemical behavior of gold (I) in dimethylsulfoxide. Electrochim Acta 95:179–184
61. Abedin SZ, Moustafa EM, Hempelmann R, Natter H, Endres F (2005) Additive free electrodeposition of nanocrystalline aluminium in a water and air stable ionic liquid. Electrochem Commun 7: 1111–1116
62. Karra S, Wooten M, Griffith W, Gorski W (2016) Morphology of AuNPs and electrocatalysis of glucose oxidation. Electrochim Acta 218:8–14
63. Erlebacher J, Aziz MJ, Karma A, Dimitrov N, Sieradzki K (2001) Evolution of nanoporosity in dealloying. Nature 410:450–453
64. Velev OD, Kaler EW (2000) Structured porous materials via colloidal crystal templating: from inorganic oxides to metals. Adv Mater 12:531–534
65. Cherevko S, Chung CH (2011) Direct electrodeposition of nanoporous gold with controlled multimodal pore size distribution. Electrochem Commun 13:16–19
66. Li W, Su B (2012) Reductive electron transfer dynamics in gold nanocluster films contacted with aqueous electrolytes. Electrochem Commun 22:8–11
67. Xiao X, Ulstrup J, Li H, Wang M, Zhang J, Si P (2014) Nanoporous gold assembly of glucose oxidase for electrochemical biosensing. Electrochim Acta 130:559–567
68. Yang XN, Huang XB, Hang RQ, Zhang XY, Qin L, Tang B (2016) Improved catalytic performance of porcine pancreas lipase immobilized onto nanoporous gold via covalent coupling. J Mater Sci 51:6428–6435
69. Yu Y, Chang S, Lee C, Wang CRC (1997) Gold nanorods: electrochemical synthesis and optical properties. J Phys Chem B 101: 6661–6664
70. Esumi K, Matsuhisa K, Torigoe K (1995) Preparation of rodlike gold particles by UV irradiation using cationic micelles as a template. Langmuir 11:3285–3287
71. Kim F, Song JH, Yang P (2002) Photochemical synthesis of gold nanorods. J Am Chem Soc 124:14316–14317
72. Wirtz M, Martin CR (2003) Template-fabricated gold nanowires and nanotubes. Adv Mater 15:455–458
73. Murphy CJ, Jana NR (2002) Controlling the aspect ratio of inorganic nanorods and nanowires. Adv Mater 14:80–82
74. Kim YJ, Song JH (2006) Practical synthesis of Au nanowires via a simple photochemical route. Bull Kor Chem Soc 27:633–634
75. Wang C, Hu Y, Lieber CM, Sun S (2008) Ultrathin Au nanowires and their transport properties. J Am Chem Soc 130:8902–8903
76. Li B, Jiang B, Tang H, Lin Z (2015) Unconventional seed-mediated growth of ultrathin Au nanowires in aqueous solution. Chem Sci 6:6349–6354
77. Chrétien S, Buratto SK, Metiu H (2007) Catalysis by very small Au clusters. Curr Opin Solid State Mater Sci 11:62–75
78. Cheng Y, Schiffrin DJ (1996) Electrodeposition of metallic gold clusters at the water/1,2-dichloroethane interface. J Chem Soc Faraday Trans 92:3865–3871
79. Girault HH, Schiffrin DJ, in Electroanalytical Chemistry (1989) ed. Bard AJ, Marcel Dekker, New York 15:1
80. Cheng Y, Schiffrin DJ (1991) Electron transfer between bis(pyridine)*meso*-tetraphenylporphyrinato iron(II) and ruthenium(III) and the hexacyanof errate couple at the 1,2-dichlor. J Electroanal Chem 314:153–163
81. Tsunoyama H, Ichikuni N, Sakurai H, Tsukuda T (2009) Effect of electronic structures of Au clusters stabilized by poly(*N*-vinyl-2-pyrrolidone) on aerobic oxidation catalysis. J Am Chem Soc 131: 7086–7093
82. Jin R, Egusa S, Scherer NF (2004) Thermally-induced formation of atomic Au clusters and conversion into nanocubes. J Am Chem Soc 126:9900–9901
83. Rodrıguez-Sanchez ML, Blanco MC, Lopez-Quintela MA (2000) Electrochemical synthesis of silver nanoparticles. J Phys Chem B 104:9683–9688
84. Rodrıguez-Vazquez MJ, Blanco MC, Lourido R, Vazquez-Vazquez C, Pastor E, Planes GA, Rivas J, Lopez-Quintela MA (2008) Synthesis of atomic gold clusters with strong electrocatalytic activities. Langmuir 24:12690–12694
85. Gonzalez BS, Rodrıguez MJ, Blanco C, Rivas J, Lopez-Quintela MA, Martinho JMG (2010) One step synthesis of the smallest photoluminescent and paramagnetic PVP-protected gold atomic clusters. Nano Lett 10:4217–4221
86. Ferrnandez-Seivane L, Ferrer J (2007) Magnetic anisotropies of late transition metal atomic clusters. Phys Rev Lett 99:183401
87. Gonzalez S (2008) Synthesis and properties of electrochemical synthesized gold atomic clusters. Master's thesis, Universidad de Santiago de Compostela, Santiago de Compostela, Spain
88. Hugentobler M, Bonanni S, Sautier A, Harbich W (2011) Morphology and stability of Au nanoclusters in HOPG nanopits of well-defined depth. Eur Phys J D 63:215–220
89. Botana J, Pereiro M, Baldomir D, Arias JE (2009) Bidimensionality of 8-atom clusters of Au: first principles study and comparison with Ag clusters. Theor Chem Account 122: 297–304
90. Dong Y, Springborg M, Warnke I (2011) Structural and thermodynamic properties of Au_{2-20} clusters. Theor Chem Account 130: 1001–1008
91. Johansson MP, Warnke I, Le A, Furche F (2014) At what size do neutral gold clusters turn three-dimensional? J Phys Chem C 118: 29370–29377
92. Johansson MP, Lechtken A, Schooss D, Kappes MM, Furche F (2008) 2D−3D transition of gold cluster anions resolved. Phys Rev A 77:053202
93. Frenke AI (2012) Applications of extended X-ray absorption fine-structure spectroscopy to studies of bimetallic nanoparticle catalysts. Chem Soc Rev 41:8163–8178
94. Bordiga S, Groppo E, Agostini G, Van Bokhoven JA, Lamberti C (2013) Reactivity of surface species in heterogeneous catalysts probed by in situ X-ray absorption techniques. Chem Rev 113: 1736–1850
95. Zhang P (2014) X-ray spectroscopy of gold−thiolate nanoclusters. J Phys Chem C 118:25291–25299
96. Li J, Lin XQ (2007) Electrodeposition of gold nanocluster s on overoxidized polypyrrole film modified glassy carbon electrode and its application for the simultaneous determination of epinephrine and uric acid under coexistence of ascorbic acid. Anal Chim Acta 596:222–230
97. Liu A, Zhu J, Han J, Wu H, Jiang C (2008) Fabrication and characterization of AuNCs on phosphorus incorporated tetrahedral amorphous carbon electrode. Electrochem Commun 10: 827–830
98. Huang SX, Ma HY, Zhang XK, Yong FF, Feng XL, Pan W, Wang XN, Wang Y, Chen SH (2005) Electrochemical synthesis of gold nanocrystals and their 1D and 2D organization. J Phys Chem B 109:19823–19830
99. Hill AC, Patterson RE, Sefton JP, Columbia MR (1999) Effect of Pb(II) on the morphology of platinum electrodeposited on highly oriented pyrolytic graphite. Langmuir 15:4005–4010
100. Li W, Wang D, Sun Q, Su B (2011) Ion transfer coupled discrete charging of immobilised AuNCs in polar organic solvents. Electrochem Commun 13:875–878
101. Anandhakumar S, Dhanalakshmi K, Mathiyarasu J (2014) Non-enzymatic organophosphorus pesticide detection using gold atomic cluster modified electrode. Electrochem Commun 38:15–18

102. Kashchiev D (2000) Nucleation basic theory with applications. Butterworth-Heinemann, Oxford
103. Budevski E, Staikov G, Lorenz WJ (1996) Electrochemical phase formation and growth. Weinheim, VCH
104. Yevtushenko O, Natter H, Hempelmann R (2007) Influence of bath composition and deposition parameters on nanostructure and thermal stability of gold. J Solid State Electrochem 11:138–143
105. Chen Y, Zeng C, Kauffman DR, Jin R (2015) Tuning the magic size of atomically precise AuNCs via isomeric methylbenzenethiols. Nano Lett 15:3603–3609
106. Aziz MA, Kim J, Oyama M (2014) Preparation of monodispersed carboxylate-functionalized gold nanoparticles using pamoic acid as a reducing and capping reagent. Gold Bull 47:127–132
107. Aziz MA, Kim JP, Shaikh MN, Oyama M, Bakare FO, Yamani ZH (2015) Size-controlled preparation of fluorescent AuNPs using pamoic acid. Gold Bull 48:85–92
108. Hill HD, Mirkin CA (2006) The bio-barcode assay for the detection of protein and nucleic acid targets using DTT-induced ligand exchange. Nat Protoc 1:324–336
109. Wei A (2004) Plasmonic nanomaterials: enhanced optical properties from metal nanoparticles and their ensembles. In: Rotello V (ed) Nanoparticles: building blocks for nanotechnology. Kluwer Academic/Plenum Publishers, New York
110. Templeton AC, Pietron JJ, Murray RW, Mulvaney P (2000) Solvent refractive index and core charge influences on the surface plasmon absorbance of alkanethiolate monolayer-protected gold clusters. J Phys Chem B 104:564–570
111. Deng J, Song Y, Wang Y, Di J (2010) Label-free optical biosensor based on localized surface plasmon resonance of twin-linked gold nanoparticles electrodeposited on ITO glass. Biosens Bioelectron 26:615–619
112. Endo HT, Takizawa Y, Imai Y, Yanagida T (2011) Study of electrical field distribution of gold-capped nanoparticle for excitation of localized surface plasmon resonance. Appl Surf Sci 257:2560–2566
113. Wang W, Wang Y, Dai Z, Sun Y, Sun Y (2007) Nonlinear optical properties of periodic gold nanoparticle arrays. Appl Surf Sci 253:4673–4676
114. D'Britto V, Sandeep CSS, Philip R, Prasad BLV (2009) Optical limiting properties of hydrophobic poly(etherimide) membranes embedded with isolated and aggregated gold nanostructures. Coll Surf A 352:79–83
115. Aziz MA, Oyama M, Reshak AH, Gondek E, Armatys P, Shebl A, Kityk IV, Wojciechowski A, Otowski W (2012) Laser stimulated optical features of AuNPs attached on ITO substrate. Phys E 44:1182–1188
116. Sun KQ, Luo SW, Xu N, Xu BQ (2008) Gold nano-size effect in Au/SiO2 for selective ethanol oxidation in aqueous solution. Catal Lett 124:238–242
117. Hashmi ASK, Hutchings GJ (2006) Gold catalysis. Angew Chem Int Ed 45:7896–7936
118. Claus P (2005) Heterogeneously catalysed hydrogenation using gold catalysts. Appl Catal A 291:222–229
119. Tsunoyama H, Sakurai H, Tsukuda T (2006) Size effect on the catalysis of gold clusters dispersed in water for aerobic oxidation of alcohol. Chem Phys Lett 429:528–532
120. Billa S, Prati L, Rossi M (2002) Selective oxidation of D-glucose on gold catalyst. J Catal 206:242–247
121. Demirel S, Lehnert K, Lucas M, Claus P (2007) Use of renewables for the production of chemicals: glycerol oxidation over carbon supported gold catalysts. Appl Catal B Environ 70:637–643
122. Haider P, Baiker A (2007) Gold supported on Cu–Mg–Al-mixed oxides: strong enhancement of activity in aerobic alcohol oxidation by concerted effect of copper and magnesium. J Catal 248:175–187
123. Abad A, Concepcion P, Corma A, Garcia H (2005) A collaborative effect between gold and a support induces the selective oxidation of alcohols. Angew Chem Int Ed 44:4066–4069
124. Inasaki T, Kobayashi S (2009) Particle size effects of gold on the kinetics of the oxygen reduction at chemically prepared Au/C catalysts. Electrochim Acta 54:4893–4897
125. Kadossov E, Burghaus U (2010) Adsorption dynamics of CO on silica supported gold clusters: cluster size effects in molecular beam scattering experiments. Catal Lett 134:228–232
126. Padayachee D, Golovko V, Ingham B, Marshall AT (2014) Influence of particle size on the electrocatalytic oxidation of glycerol over carbon-supported gold nanoparticles. Electrochim Acta 120:398–407
127. Ivanova OS, Zamborini FP (2010) Electrochemical size discrimination of gold nanoparticles attached to glass/indium-tin-oxide electrodes by oxidation in bromide-containing electrolyte. Anal Chem 82:5844–5850
128. Masitas RA, Zamborini FP (2012) Oxidation of highly unstable <4 nm diameter gold nanoparticles 850 mV negative of the bulk oxidation potential. J Am Chem Soc 134:5014–5017
129. Plieth WJ (1982) Electrochemical properties of small clusters of metal atoms and their role in the surface enhanced Raman scattering. J Phys Chem 86:3166–3170
130. Haruta M (2004) Gold as a novel catalyst in the 21st century: preparation, working mechanism and applications. Gold Bull 37:1–2
131. Pyykko P (2004) Theoretical chemistry of gold. Angew Chem Int Ed Engl 43:4412–4456
132. Ulman A (1996) Formation and structure of self-assembled monolayers. Chem Rev 96:1533–1554
133. Bond GC, Louis C, Thompson DT (2006) Catalysis by gold. Imperial College Press, London
134. Liua XY, Wang A, Zhang T, Mou CY (2013) Catalysis by gold: new insights into the support effect. Nano Today 8:403–416
135. Rezende TS, Andrade GRS, Barreto LS, Costa NB, Gimenez IF, Almeida LE (2010) Facile preparation of catalytically active gold nanoparticles on a thiolated chitosan. Mat Lett 64:882–884
136. Eremenko AM, Smirnova NP, Mukha IP, Yashan HR (2010) Silver and gold nanoparticles in silica matrices: synthesis, properties, and application. Theor Exp Chem 46:65–88
137. Das M, Shim KH, An SSA, Yi DK (2011) Review on gold nanoparticles and their applications. Toxicol Environ Health Sci 3:193–205
138. Majdalawieh A, Kanan MC, El-Kadri O, Kanan SM (2014) Recent advances in gold and silver nanoparticles: synthesis and applications. J Nanosci Nanotechnol 14:4757–4780
139. Kang HJ, Patra S, Das J, Aziz A, Jo J, Yang H (2010) Effect of aging on the electrocatalytic activity of gold nanoparticles. Electrochem Commun 12:1245–1248
140. Burke LD, O'Connell AM, O'Mullane AP (2003) The role of defects, or active states, in surface electrochemistry with particular reference to gold in neutral solution. J Appl Electrochem 33:1125–1135
141. Das J, Patra S, Yang H (2008) Enhancement of the electrocatalytic activity of gold nanoparticles via $NaBH_4$ treatment. Chem Commun 37:4451–4453
142. Saldan I, Burtovyy R, Becker H, Ader V, Wöll C (2008) Ti-Ni alloys as MH electrodes in Ni-MH accumulators. Int J Hydrog Energy 33:7177–7184
143. Saldan I, Frenzel J, Shekhah O, Chelmowski R, Birkner A, Wöll C (2009) Surface of Ti-Ni alloys after their preparation. J Alloy Comp 470:568–573
144. Saldan I (2010) Primary estimation of metal hydride electrode performance. J Solid State Electr 14:1339–1350
145. Guo S, Wang E (2007) Synthesis and electrochemical applications of gold nanoparticles. Anal Chim Acta 598:181–192
146. Gopalan AI, Lee KP, Manesha KM, Santhosh P, Kim JH (2006) Gold nanoparticles dispersed into poly(aminothiophenol) as a

novel electrocatalyst—fabrication of modified electrode and evaluation of electrocatalytic activities for dioxygen reduction. J Mol Catal A 256:335–345
147. Etesami M, Mohamed N (2011) Catalytic application of gold nanoparticles electrodeposited by fast scan cyclic voltammetry to glycerol electrooxidation in alkaline electrolyte. Int J Electrochem Sci 6:4676–4689
148. Ahammad AJS, Choi YH, Koh K, Kim JH, Lee JJ, Lee M (2011) Electrochemical detection of cardiac biomarker troponin I at gold nanoparticle-modified ITO electrode by using open circuit potential. Int J Electrochem Sci 6:1906–1916
149. Guoa S, Wang E (2011) Noble metal nanomaterials: controllable synthesis and application in fuel cells and analytical sensors. Nano Today 6:240–264
150. Guo SJ, Wen D, Zhai YM, Dong SJ, Wang EK (2010) Platinum nanoparticle ensemble-on-graphene hybrid nanosheet: one-pot, rapid synthesis, and used as new electrode material for electrochemical sensing. ACS Nano 4:3959–3968
151. Huang J, Wang D, Hou H, You T (2008) Electrospun palladium nanoparticle-loaded carbon nanofibers and their electrocatalytic activities towards hydrogen peroxide and NADH. Adv Funct Mater 18:441–448
152. Razzaq H, Qureshi R, Schiffrin DJ (2014) Enhanced rate of electron transfer across gold nanoparticle-anthraquinone hybrids. Electrochem Commun 39:9–11
153. Schiffrin DJ (2017) Current topics in physical and nanoparticle electrochemistry. Cur Opin Electrochem. https://doi.org/10.1016/j.coelec.2017.08.012
154. Wei H, Li B, Li J, Dong S, Wang E (2008) DNAzyme-based colorimetric sensing of lead (Pb^{+2}) using unmodified gold nanoparticle probes. Nanotechnology 19(5):095501
155. Li D, Wieckowska A, Willner I (2008) Optical analysis of Hg^{2+} ions by oligonucleotide-gold-nanoparticle hybrids and DNA-based machines. Angew Chem Int Ed 47:3927–3931
156. Wang H, Wang Y, Jin J, Yang R (2008) Gold nanoparticle-based colorimetric and "turn-on" fluorescent probe for mercury(II) ions in aqueous solution. Anal Chem 80:9021–9028
157. Wei H, Li BL, Li J, Wang EK, Dong SJ (2007) Simple and sensitive aptamer-based colorimetric sensing of protein using unmodified gold nanoparticle probes. Chem Commun 43:3735–3737
158. Lv ZZ, Wei H, Li BL, Wang EK (2009) Colorimetric recognition of the coralyne-poly(dA) interaction using unmodified gold nanoparticle probes, and further detection of coralyne based upon this recognition system. Analyst 134:1647–1651
159. Zhang J, Wang L, Pan D, Song S, Boey F, Zhang H, Fan C (2008) Visual cocaine detection with gold nanoparticles and rationally engineered aptamer structures. Small 4:1196–1200
160. Jiang Y, Zhao H, Lin Y, Zhu N, Ma Y, Mao L (2010) Colorimetric detection of glucose in rat brain using gold nanoparticles. Angew Chem Int Ed 49:4800–4804
161. Staszak-Jirkovský J, Ahlberg E, Panas I, Schiffrin DJ (2016) The bifurcation point of the oxygen reduction reaction on Au–Pd nanoalloys. Faraday Discuss 188:257–278
162. Penon O, Marín MJ, Russell DA, Pérez-García L (2017) Water soluble, multifunctional antibody-porphyrin gold nanoparticles for targeted photodynamic therapy. J Coll Interface Sci 496:100–110